Finite Element Investigation of Closed Head Injuries

By

Hongxi Chen

A thesis submitted to
the Faculty of Graduate Studies
in partial fulfilment of
the requirements for the degree of
Master of Science

Department of Mechanical and Manufacturing Engineering
Faculty of Engineering
University of Manitoba
Winnipeg, Manitoba

July 2010

Abstract

Head injuries are very common in daily life and in war field. Head injuries are classified into open and closed. The mechanical mechanisms involved in closed head injuries are very different from those in open head injuries. Closed head injuries are more often reported with the use of protective device such as helmets. Helmets were found effective in reducing open head injuries, but less effective for closed head injuries.

Finite element modeling is an effective and efficient tool for investigating head injuries. In this thesis, a two-dimensional finite element model was constructed based on a Magnetic Resonance Image (MRI) scan data from a patient. MATLAB programming was used to extract the information from the MRI scan data. The finite element model was then used to investigate factors affecting closed head injuries. As a new contribution to closed head injury study, the fluid component in the human head, CSF, was studied by a group of comparative simulations. The other three factors, elasticity modulus of the cranium, contact area of impact, and impact duration were also investigated. Their effects on reducing the strain values in the brain were measured.

Investigation results show that, increasing elasticity modulus of the cranium, contact area of impact and impact duration are very helpful to reduce the strain values in the brain. Helmet is helpful to protect people from closed head injuries because it can change all these three factors by using different shell stiffness and different padding material. The cerebrospinal fluid is effective in protecting the brain from impacts, as a fluid is able to

reduce normal strains and filter nearly all shear strains transferred to the brain. It indicates that if a layer of fluid could be added as a layer in a protective helmet, the helmet would be more effective in protecting the brain. Conclusions obtained from the investigations are helpful for preventing closed head injuries and for improving design of protective devices such as helmets.

Acknowledgments

To Dr. Y. Luo，my MSc supervisor, I would like to express my sincere gratitude. It was my privilege to be his graduate student and I am so proud to be one of his graduate students. I appreciate his guidance in this research, and his help on my English writing. I express my appreciation and deep gratitude for his support, guidance, and advice.

I also want to thank Prof. Q. Zhang. I obtained my theoretical and experimental knowledge on biological materials from his course. It was very helpful to my research.

Thanks must be given to my friends Caixia, Xiumei, Nan, Santosh, and Qianqiu. They gave me the unconditional love, support, encouragement and help during the courses of my MSc study.

I extend my gratitude to Manitoba Medical Service Foundation (MMSF) for the awarded grant supporting the reported research.

Contents

List of Tables

List of Figures

List of Abbreviations

CHI	Closed Head Injury
CSF	Cerebrospinal Fluid
CT	Computed Tomography
DAI	Diffuse Axons Injury
FEA	Finite Element Analysis
FEM	Finite Element Method
HI	Head Injury
MR	Magnetic Resonance
MRI	Magnetic Resonance Image
MRE	Magnetic Resonance Elastography
TBI	Trauma Brain Injury

List of Symbols

ρ_s	mass density of solid material
σ_x, σ_y	normal stresses in *x*, *y* direction
τ_{xy}	shear stress
u_x, u_y	the displacement in *x*, *y* directions
∇	the differential operator
$\boldsymbol{\sigma}$	the stress tensor
c	sound speed of in a fluid medium
p	acoustic pressure
t	time variable
∇^2	Laplace operator
$[M^S]$, $[M^f]$	the mass matrix of solid domain, fluid mass matrix
$[K^S]$, $[K^f]$	the stiffness matrix of solid domain, fluid domain
$[C^S]$,$[C^f]$	damping matrix of viscoelastic solid domain, the fluid damping matrix

N_u	element shape functions for displacements
$[B_u]$	*B*-matrices
$\{L\}$	matrix operator
$\{F_f\}$	load vector
D	material property matrix for the solid parts
Ω_s , Ω_f	sub-domains occupied by the solid and the fluid
S	interface surface between the solid parts and the fluid.

Chapter 1

Introduction

1.1 General description of head injury

The technical definition of head injury (HI) refers to damage to any part of the head. It can range from a minor surface bump on the scalp or face to fatal brain injuries. Among all head injuries, brain injury, or Trauma Brain Injury (TBI), is the most fatal one. A brain injury usually leads to physiological and cognitive dysfunctions. There are many symptoms that can be resulted from a head injury. The brain is the biological, physiological and mental control center for the whole human body; therefore, any damage to the brain will affect the functionalities of all parts of the body. Symptoms of HI are divergent due to the different locations of the human body affected. Patients may feel dizziness, headaches, nausea, etc. Some severe HI patients could suffer from various dysfunctions including the ability to control emotions and to interact socially, vision and equilibrium problem, physical disabilities and even coma. The most common causes of head injuries

include: car accidents (passenger and pedestrian), bicycle/motorcycle accidents, falls (especially children and the elderly), sports injuries, and violent assaults.

1.2 Survey on head injury

Surveys are quite helpful for revealing characteristic phenomena of HI, and also useful for providing persuasive data for studying efficiency of HI protection devices. From the surveys conducted in the literature, it is found that HI is one of the most serious public health problems with particularly high incidence and mortality, causing great economic loss. HI occurs extremely frequently in daily life, working places and in sports. As noted from the surveys carried out in the United States [1, 2]，approximately every 21 seconds a person has a head injury. Annual HI incidence in US is around 180-250 per 100,000 people. This number is even higher in developing countries such as China, India and South Africa. Each year in the US,

- More than 500,000 people are hospitalized due to head injuries;
- Among the above people, 75,000-100,000 head injuries are fatal;
- 70,000-90,000 survivors of head injuries are irreversible with lifelong disabilities and dysfunctions;
- 2,000 survivors of head injuries live in a vegetative state for the rest of their lives.

The direct medical costs for treatment including hospitalization, acute care and various rehabilitation services are estimated $48.3 billion per year. In overall HI is decreasing as suggested by the surveys over the past several decades [1], but it is still considerably high. As far as the US concerned [3], HI accounts for approximately 40% of all deaths from acute injuries. More recent survey on HI mortality rates (per 100,000 people) per year from different regions of the world are listed in Table 1.

Table 1 HI mortality rates in different regions [1]

Country/Region	Europe	Scandinavia	India	U.S.	Taiwan, China	South Africa	Colombia
Mortality rate	15	10	20	30	38	81	120

The decrease in HI mortality in recent years is probably the result of a combination of several factors. Protection devices such as safety belts, air bags, safety helmets have played a very important role. Motorcycle helmet, for an example, reduced motorcycle-related death by 29% during 1972-1987, while during 1993-2000 the reduction was further increased to 37% possibly due to improvement in helmet design and advances in materials [3]. However, road traffic accidents are still the biggest contributor to the mortality rate of head injuries. Based on the surveys done by Injury Surveillance, Health Canada and Road Safety in 2001, nearly every minute one person is killed by a traffic accident,

and approximately 70% of the deaths were due to head injuries [4]. Therefore, there is a need to fully reveal the intrinsic mechanisms of HI to reduce the incidence and mortality. Furthermore understanding the mechanisms of HI is an initial step for improving the design of protective devices.

1.3 Classification of head injury

For the purpose of more effectively investigating the involved mechanical mechanisms, head injuries are classified as open (penetrating) head injuries and closed (non-penetrating) head injuries. An open (penetrating) head injury refers to a head injury involving damages of the skull. While a closed head injury (CHI) refers to a traumatic brain injury without any or minor skull fracture or loss of continuity of mucous membranes.

In an open head injury, the skull is usually pierced or fractured by a sharp foreign object such as a bullet with a large impulse force. In an open head injury, the integrity of the skull and the brain is usually severely damaged. Open head injuries can be protected effectively by using helmets. A helmet can protect the skull form being penetrated by a sharp object, as it is able to uniformly distribute the impact force to the skull. Furthermore, a helmet is also designed to absorb part of the impact energy. However, fatal HI may occur without any damage to the skull. For the widely use of protective devices such

as helmets, more and more CHI incidences have been reported. For instance, in motorcycle accidents, CHI is more common than open head injury. Protective devices such as helmets that can provide more effective protection against CHI are still under research and development. During an impact, kinetic energy that is not absorbed by the helmet and the skull will be transferred to the brain. Relative motion between the skull and the brain is thus introduced. Due to the relative motion, the brain will have collision with the skull. Brain tissues having different material properties may also have relative motion between them. If the strains and stresses in the brain tissues exceed the material strength of the blood vessels and the nerve fibres, intracranial bleeding will occur. As the blood from the broken vessel is forced to seep into the brain tissue, the brain may start to swell and intracranial pressure will increase. The nerve may be damaged permanently which may lead to a vegetative state or coma.

1.4 Types of closed head injuries

From the pathological point of view, closed head injuries can be classified into diffuse brain damage, localized brain contusion and coup-contrecoup brain injury.

- Diffuse brain damage [5]

In diffuse brain damage, brain dysfunctions are caused by hypoxia, damage to blood vessels and axon system. Concussion is a very common mild diffuse brain damage, which will affect normal brain functions temporarily. While Diffuse Axons Injury (DAI) is a common severe diffuse brain injury. DAI refers to widespread damage to white matter where cerebral axons locate. Axon is a long and thin neural path that allows neuron to communicate with each other. DAI will lead to permanent damage to nerves system in the brain. Severe DAI causes vegetative states or comas in 90% of patients.

- Localized brain contusion[6]

In localized brain contusion, bruise of brain tissue is localized, and symptoms are usually related to the damaged area of the brain. Additionally, blood vessels are very likely to rupture in localized brain injury, resulting collection of blood outside of blood vessels in the brain or in between the brain and skull. It can cause permanent neurological damage while blood is absorbed into cerebrospinal fluid. Brain contusion could also develop to haemorrhages when blood is absorbed into brain tissue, which may lead to unconsciousness, seizures and/or lethargy.

- Coup and contrecoup contusion [7, 8]

Coup and contrecoup contusion is a very special phenomenon in CHI. It has been frequently observed in clinics. It was found that coup-contrecoup brain injury is dominantly located at coup side (impacted side) and contrecoup side (the opposite of the impacted site). In some cases injury at the contrecoup site is even more severe than that at the impact site (coup injury).

Mechanical force is regarded as a very important aspect affecting patterns of head injuries. Based on clinical and experiment investigations, there is considerable correlation between impact force and head injury types. Most diffuse injuries such as brain concussion, subdural hematoma and diffuse axonal injuries are resulted from large acceleration or deceleration motion, which is also called inertial loading. A special diffuse injury needs to be noted is the baby shaking syndrome, which is caused by violently shaking of an infant [9]. Most localized brain contusions and epidural hematoma are caused by direct impact [10]. In most real-world head injuries, the causal forces causing a brain injury are usually a combination of inertial force and impact. Functional and traumatic damage of brain is difficult to quantify.

But mechanical mechanism of coup-contrecoup phenomenon has not been completely clarified due to its great complexity. There are a number of theories proposed to explain this phenomenon. Among them the most popular ones are the positive pressure theory,

the negative pressure theory, the cerebrospinal theory, and the shear strain theory [11, 12, 13]. In the positive pressure theory, it is assumed that if the head is experiencing an acceleration or deceleration, the motion of the brain tends to lag behind the skull. As a result, the brain is compressed against the skull at the contrecoup location. Meanwhile all the cerebrospinal fluid is pushed to the coup site. If the head is bumped by an object, a positive pressure wave amplifies the existing compression, which further pushes the brain tissue against the skull at the contrecoup location and causes the contrecoup injury [11]. The negative pressure theory, presented by Russell, suggests that the brain continues to move forward once the skull is suddenly stopped at a bump. Hence there will be tensile stress developed at the contrecoup site (negative pressure). This tensile stress is increasing during the impact, and eventually leads damage to brain tissue, axonal system or vessels at the contrecoup side [12]. In the CSF theory it assumes that CSF is denser than brain tissue. Thus, the brain at impact is propelled to the contrecoup location due to the CSF moving forward towards the coup site [13]. Shear strain theory is based on two observations: brain tissues are almost incompressible; and brain tissues have much lower shear modulus. It is believed shear strain is the dominant reason of coup-contrecoup brain injuries. However, none of these theories could explain coup-contrecoup problem satisfactorily.

These theories are not supported by simulation results [8], and some of them do not conform to clinic observation [4].

Biomechanics of CHI need to be well understood to protect people from head injuries. It is the first step to improve the effectiveness of protection devices, and it is also important for injury diagnose and treatment.

1.5 Available methods for studying head injuries

Great effort has been made to study mechanics of head injuries since its inception in 1939 in the United States [14]. Methodologies used in head injury research could be grouped into physical experiments, analytical methods and numerical simulations.

1.5.1 Physical experiment

Physical experiment is one tool for investigating head injuries. It is a direct way to obtain material properties of the human head. Considerable amount of physical experiments have been done to investigate mechanical behaviours of components in the head such as skull, brain tissues, vessels etc. Samples of human and animal cranial bones have been tested under tension, compression, simple shear, and torsion in [15, 16]. Mechanical behaviors of brain tissues have been tested mostly in vitro by shearing [17, 18], compres-

sion [19, 20] and tension [21, 22]. Brain tissues were also studied by observing the response of in vivo porcine brain tissues under mechanical forces [23]. Physical experiments were also carried out to study mechanical properties of blood vessels. For instance, longitudinal stress-strain behavior of human cerebral vessels major cerebral arteries were tested in [24]. Material properties of cerebral aneurysms and human parasagittal bridging veins have also been tested under various strain rates and loading conditions [25, 26]. Furthermore, experimental investigations provide evidence to validate analytical and numerical models. Analytical and numerical models are constructed and improved by comparing data collected from physical experiments [27, 28]. Additionally, physical experiments are also used to determine injury tolerance and thresholds for skull and vessel failure, brain and brainstem damage, etc [29, 30]. These tolerance and threshold values are very important to establish head injury criterion. The values are also essential for designing protective devices.

However, physical experiments also have a number of difficulties and limitations for studying brain injuries. Only small minority of controlled head testing employing non-injurious levels load can be conducted in reality, while harmful physical experiments are strictly forbidden on living human body. Recently, lots of in vivo animal tests are also restricted by legislations [4]. Cadavers and live or anaesthetized animals are commonly

used as a surrogate for mechanical tests. But physical conditions of living human body are different from cadavers. Based on clinical observations, blood stops circulating and body fluid is completely absorbed into brain tissues after death. Brain tissues in cadaver are much harder than those in vivo.

1.5.2 Analytical method

Analytical method is another method used to study head injuries, mainly for the purpose of reducing the amount of physical experiments. But it only can be used for qualitative study to head injuries because of its limited ability to deal with complicated problems [4]. In a procedure for obtaining explicit solution, simplifications on geometry and material have to be introduced into the model. The human head usually has to be idealized as a uniform structure with regular shape in analytical methods.

1.5.3 Numerical simulations

In recent decades, numerical simulations are more and more extensively employed to study head injuries. Advances in computer capacity have made it possible to deal with more and more complex models. Numerical methods are mainly represented by the Finite Element Method (FEM) [4]. FEM is a numerical technique for finding approximate solu-

tions over complicated domain. FEM is regarded as one of the most powerful tools which have been applied in biomechanical analysis and especially in head injury studies. FEM is able to deal with problems having complex geometry and complicated material properties such as the human head.

Compare to physical experiments, numerical simulations have the following advantages:

- In numerical simulations, the head model can be subjected to and extreme loading conditions. Various impact conditions can be simulated, which may be difficult and even impossible to implement in physical experiments.
- Complex experiment conditions are able and much easier to achieve in numerical simulations. While in real physical models, high technology and professional equipments are required to apply excitations, detect and record responses.

Considerable finite element investigations on head injuries have been conducted during the last two decades. Objectives of these finite element investigations are mainly focused on the following four aspects [4]:

- Predict the response of human head under impacts, including the deformation of the skull, the maximum pressure, maximum stress, shear stress in the brain tissue [8, 31, 15, 32];
- To establish and to improve head injury criterion (HIC) [33];

- To design mode effective protective device[34, 35];
- To diagnose injury or pathological change in human brain in a noninvasive way.

Finite element modeling of the human head has presented as a gradual progress. In early 1970's, three dimensional models had been constructed to study intracranial mechanical responses. However, these models were usually simplified into regular geometries such as cylindrical, spherical, or ellipsoidal shells [36, 37]. The materials of the human head were modeled as a linearly visco-elastic soft core bonded by a linearly elastic hard shell [37]. While in the 1980's, more details within the cranium was able be included due to non-invasive imaging technology such as computer tomography (CT). It leaded a great development in Finite element modeling of the head.

Currently finite element modeling of the human head is still challenging due to its extremely complexities in geometry and material properties. There are three models that can be considered as milestones in finite element modeling of human head. The first one is the model constructed by Ward [38]. It is a brain model with very detailed intracranial structures including cerebrum, cerebellum, brain stem, ventricles and dural membrane. The brain model was repeatedly refined to match the experimental data from cadavers. This is one of the very few models which could match with real cadaver tests. But the model did not include the skull, which limited its applications to only inertial loading.

The second model is a very detailed three-dimensional head model constructed by Hosey and Liu [39]. It included the three-layered skull, scalp, CSF, spinal cord and the cervical spinal column. But the capability of this model was not fully evaluated owing to its complexity as well as the limitation in the computer facility and analysis software [39]. The last one is a detailed head model which could be used for nonlinear dynamic analysis. In the model, the skull, brain and CSF were discretised to eight-node hexahedron elements. The scalp, dural mater and falx cerebrum were represented as four-node thin shell elements [40].

Current technologies allow constructing more and more advanced finite element models that are more faithful to the real prototype. Technically speaking, it is possible to establish a finite element model that is completely faithful to the real human head, as long as detailed geometrical information and material properties are available. But the information, especially the material properties, is still unavailable, because the human head has very complex anatomical structure. The human head consists of many macro and micro anatomical components including white mater, grey mater, blood vessels, axons, cerebral fluid, etc. Due to the limitations of currently available experiment methods, it is very difficult and even impossible to obtain the in vivo material properties of these components,

as any test is required to be harmless to a living human. Thus obtaining precise and detailed material properties of human is a big challenge to head injury research.

1.6 Objective of this thesis

The objective of this thesis is to understand mechanical mechanisms involved in closed head injuries and to provide guidance for improving protective helmets, by investigating the effects of the following aspects on closed head injuries using finite element modeling.

- Role of cerebrospinal fluid (CSF) in protecting the brain

  The space between skull and the brain is fulfilled with CSF. But in most previous research, CSF was usually ignored or over simplified as a solid for the convenience of numerical solution. Only in some recently reported limited research, CSF is considered as a fluid. For instance, CSF is considered as an incompressible fluid described by the Navier-Stokes equations in the study of the mechanism of coup-contrecoup phenomenon [8]. By studying blast-induced intracranial wave physics leading to a head injury [41], it was known that CSF can be assumed as an incompressible fluid. However, knowledge about effect of CSF in head injuries is quite limited. In the research reported in this thesis, it was aimed to reveal the role of CSF by finite element modeling, for example, how effective is CSF in buffering the brain against the skull,

and how does CSF affect strain fields in the brain during an impact. Hopefully the investigation would provide useful information for refining finite element modelling of the human head.

- Cranial Young's modulus

  Young's modulus of the skull also plays a significant role in head injuries. Cranial Young's modulus changes notably with age. This is why head injury incidences are age-related. As evidenced by population-based surveys carried in many different regions including France, Olmsted County, San Diego, Australia, North Manhattan, similar results have been obtained: head injury incidence is the highest among infants and youths [1]. Cranial Young's modulus of youths and infants are much smaller than that of adults. How cranial Young's modulus affects head injuries was investigated by finite element modeling.

- Impact contact area and impact duration

  Increasing the contact area of impact is considered as one of the most effective ways to protect both closed and open head injuries. It is also the primary protection mechanism of helmets. Distribution of impact load will definitely reduce stress concentration in the skull, but its benefit to brain needs further evaluation.

The protective gears such as helmets are also able to change impact duration by using different padding material. It is believed that increasing of impact duration also helps to alleviate the damage to brain during a strike. Its quantitative effect no brain injuries also needs further investigation.

In Chapter 2, a brief introduction to anatomical structure of the human head is presented, for a better understanding on the mechanical role of each component. Then, in Chapter 3, we construct our finite element model of the head, and establish the governing equations for the motion of each component and their interaction. In Chapter 4, results of the simulations are presented and discussed. Concluding remarks and future works are described in Chapter 5.

Chapter 2

Anatomical Structure of Human Head

Anatomical structure of the human head is introduced in this chapter. A finite element model is constructed based on the anatomical structure of the head. For the purpose of investigating mechanical mechanism of head injuries, the skin, face muscles, scalp and hairs are not considered at this stage of research. As shown in Fig.1, the major components of the head are the brain, the skull and CSF between them. Roughly speaking, skull is a hard outer shell, and brain is soft and delicate tissues suspending by the liquid CSF in skull.

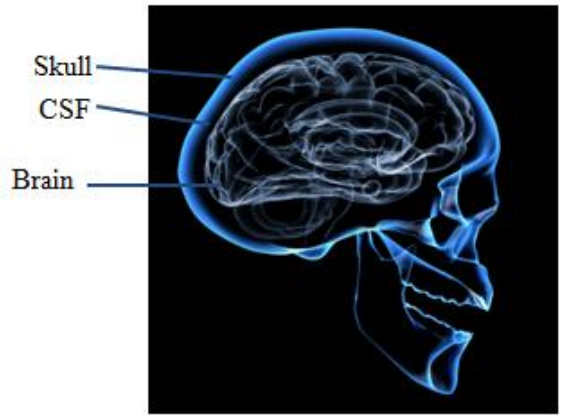

Figure 1 Anatomical structure of human head [42]

2.1 The Skull

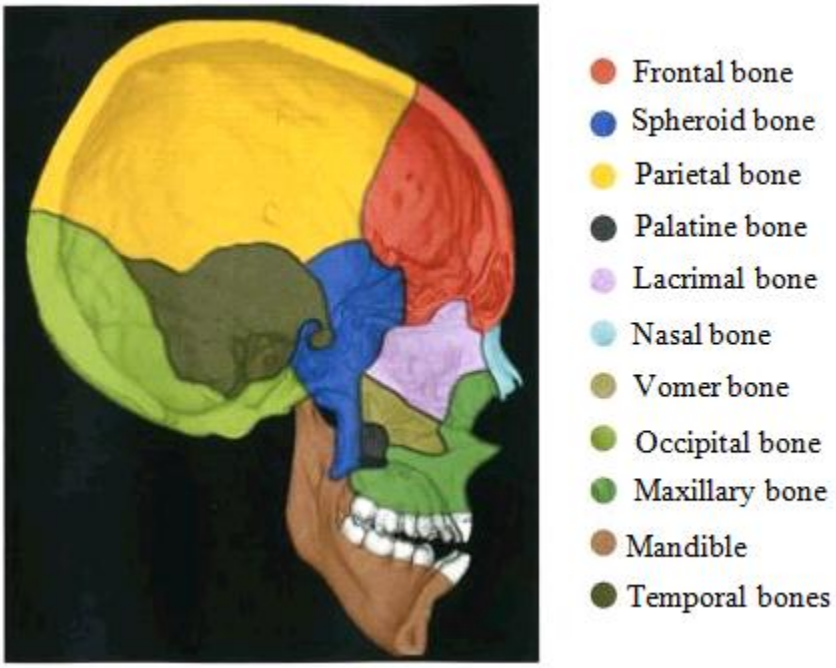

Figure 2 Structure of human skull [43]

The skull is a bony structure composed of a number of pieces of bones as shown in Figure 2. These cranial bones are connected by articulations such as sutures and joints. The articulations have irregular shapes and their strength change significantly with age. The skull of newborns consists of thin, flexible plates. Partially calcified bony tissues join at plate margins by patent, membranous sutures, which are vulnerable to impacts and squeezing forces [44, 45]. For the adults, the suture has similar strength as the cranial bone; while for the kids, the suture has much lower strength than the cranial bones. It is the direct reason why head injuries are more frequently occurred among the children.

From a mechanical point of view, the cranium can be seen as a protection container in which the intracranial content neatly fits. Both interior and exterior surfaces of skullcap are non-uniform and discontinuous.

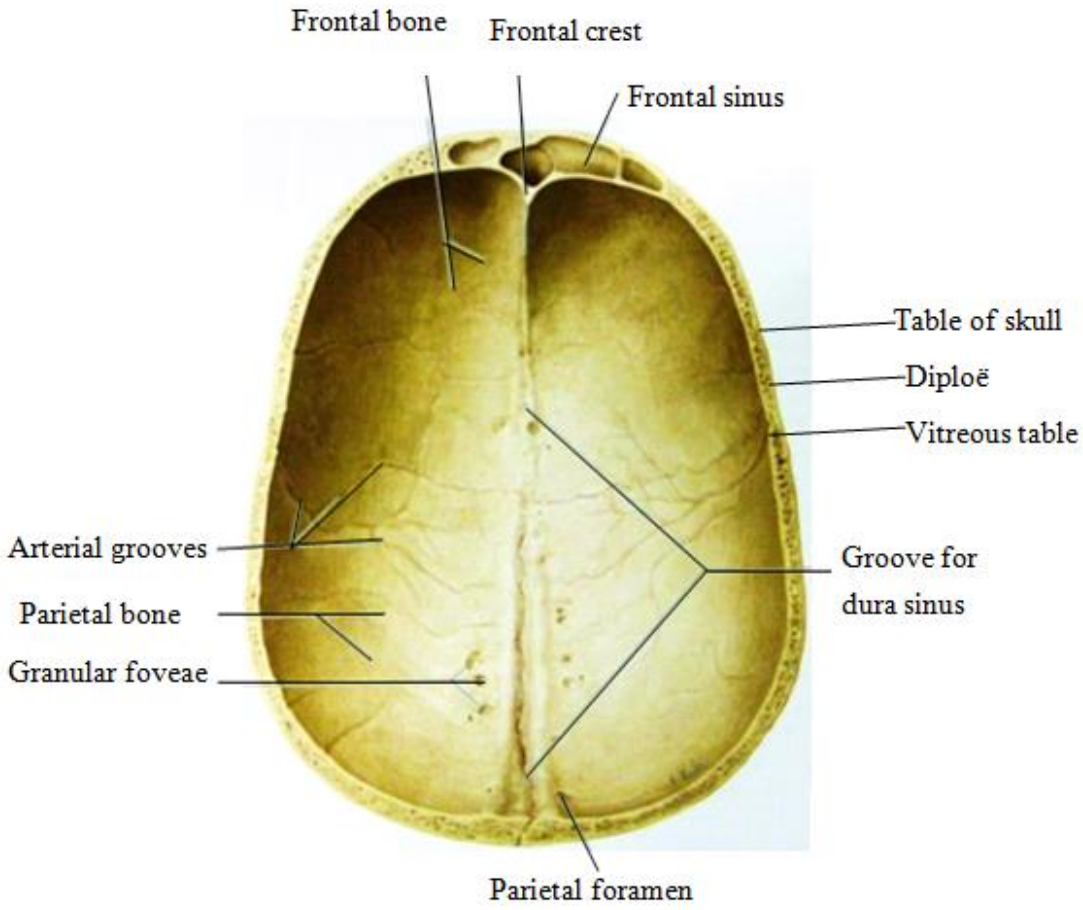

Figure 3 Cranium [46]

Figure 3 shows the inner side of cranium. The cranium is composed of a frontal bone, two parietal bones and a small occipital bone. The inner surface of skull is quite rough. There are irregular shaped crests. The surface also has depressions such as groove, foveae, sinus corresponding to the cerebral convolutions, and numerous furrows for the ramifica-

tions of various blood vessels [46]. Moreover, the thickness of the cranium varies in the range of 0.2cm to 1.0cm. The skull geometry may play a role in head injuries by affecting strain and stress distributions. The uneven surface might lead to dramatic strain or stress concentration, and potentially cause substantial strains and stresses in the nerves and brain tissues connected to them. Cranial bones have very special sandwich structure as shown in Figure 3. A cranial bone has two tables of compact bones, the outer and inner plates, and sponge bone filled between called diplo ë [46]. Thickness and density of diplo ë vary significantly with the subject age. Material properties of the skull, including the density, energy absorption, gross stiffness and damping coefficient, are affected by the micro-structure of the diplo ë

Based on material properties obtained by physical experiments, the three layers of the skull can be approximately considered as linear elastic and isotropic materials under small loading [14], as evidenced by a set of tensile stress-strain curves shown in Figure 4.

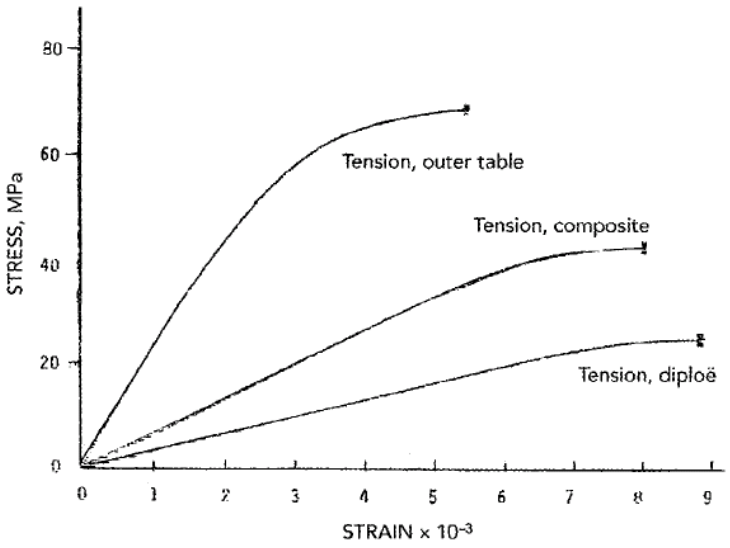

Figure 4 Quasi-static tensile stress-strain curves of human skull: outer table, composite, and diplo ë[14]

2.2 The Brain Tissue

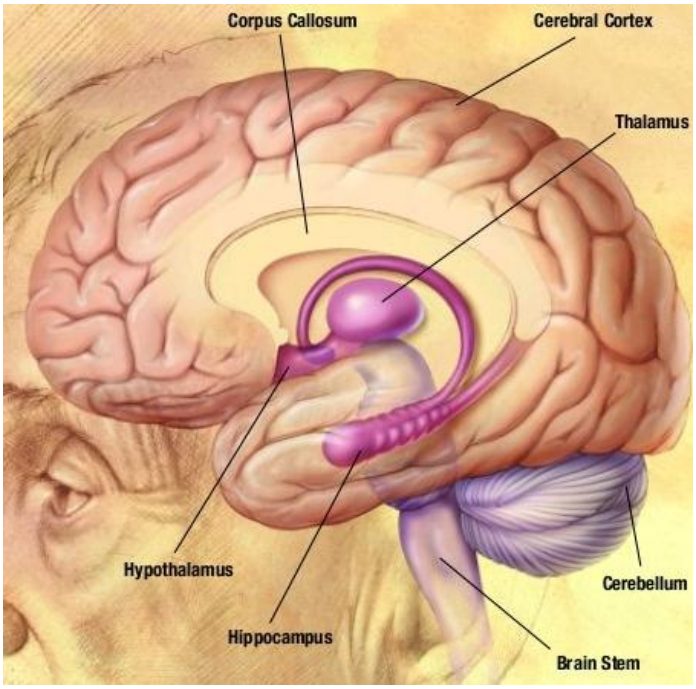

Figure 5 Major parts of the human brain [47]

The human brain consists of cerebral cortex, cerebellum, brain stem, thalamus, corpus callosum, hippocampus and hypothalamus, see Figure 5. The mass of an adult's head is about 4.5kg, of which the brain is about 1.5kg [46]. As shown in Figure 3, brain has curved and irregular geometry. Brain tissues are arranged into a number of folds. There is lots of deep sulcus on the brain surface.

In brief, from mechanical point of view, brain tissue is highly heterogeneous two-phase material. There are a great amount of brain vessels and nerves embedded inside brain tissue. Different kinds of membranes serve as barrier between different phases. Blood is pumped into the brain and circulating through it. Cerebrospinal fluid flows throughout the inner ventricular system in the brain and is absorbed back into the bloodstream, rinsing the metabolic waste from the central nervous system (CNS) through the blood-brain barrier.

Brain tissues present distinctive mechanical properties. Considerable amount of research has been done aiming at characterizing brain tissue properties. Mechanical behaviour of brain tissues under external force may vary by an order of magnitude as reported in [48]. In some experiments it was observed that brain tissue has very low elasticity modulus and high yield strains, similar to elastomers [49]. It is also arguable if, or not, brain tissues can be treated as a nearly incompressible, capable of permanent deformation and nonlin-

ear rubber-like material [49]. Experiment results exhibit huge diversities, possibly due to differences in equipments, donor samples and test methods employed in the experiments.

It is generally agreed that brain tissues are viscoelastic, heterogeneous and anisotropic [48, 19]. Based on data from in vitro tension and compression tests of swine brain tissues [19, 22, 50], brain tissues can be considered as a hyper-viscoelastic material. Stress-strain curves obtained from all tensile tests are in the shape of downward convex under different loading rates. It was also found that stress-strain relation of brain tissue is strongly rate dependent. Brain tissue behaves much stiffer under higher loading rate. Stiffness of brain tissue under compression or tension is different. Swine brain tissue was found to be considerably softer in tension than in compression.

There is no consensus on what material model is generally applicable for brain tissues [48], but it was proposed that for small strains the linear, viscoelastic material model should be adequate [50].

What should be noted in the experiments is that the brain tissue samples tested include nerves and brain vessels. Thus, the reported material properties are actually a combination of material properties from brain tissues, blood vessels and nerves.

2.3 The Meninges and Cerebrospinal Fluid (CSF)

The brain is covered by three layers of membranes called Meninges that are located between the brain and the skull. Thin film of fluid, called cerebrospinal fluid (CSF), fills the space between the membranes [46]. Meninges, especially CSF, provide protections to the brain.

2.3.1 The Meninges

Meninges consist of three membranes, dural matter, arachnoid matter and pia matter from outside to inside as shown in Figure 6. Dura matter is a durable membrane composed of two layers: periosteum and meningeal. It attaches to the skull and contains many blood vessels. Arachnoid membrane is the middle layer, which is a thin, transparent membrane and composing of fibrous tissue. Pia matter is a very delicate membrane which firmly adheres to the surface of the brain and follows all the minor contours of the brain [46].

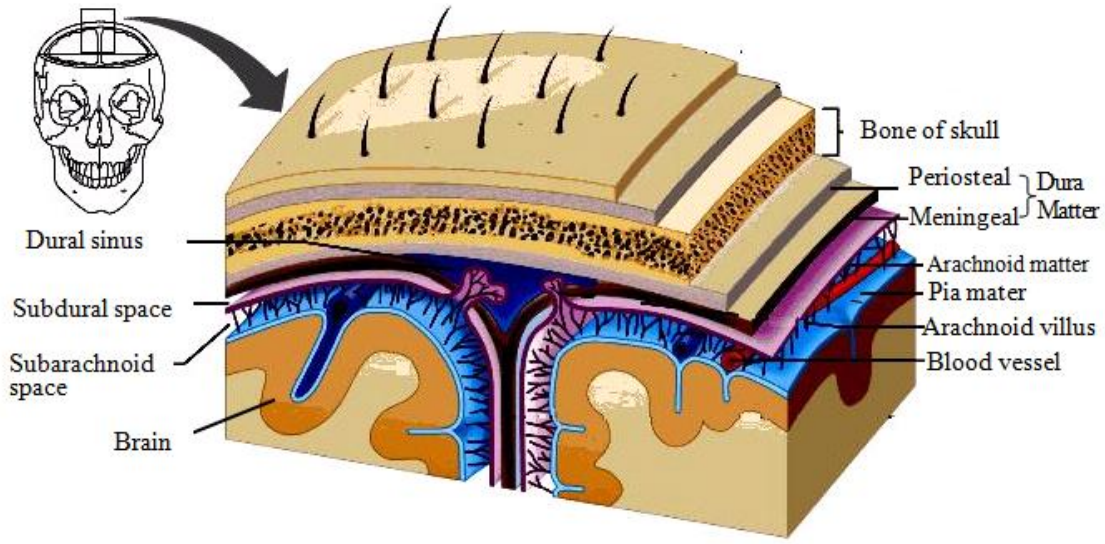

Figure 6 Structure of meninges [51]

Two layers of spaces exist between the membranes. They are called subdural space and subarachnoid space, respectively, as shown in Figure 6. For head injuries, one common symptom is subdural bleeding. The dural mater contains blood vessels. Breakage of these vessels would lead to subdural bleeding. Blood clots will be formed consequently. It is clinically termed subdural haematoma. The formed blood clots would fill the subdural space and compress the underlying neural system. The subarachnoid space contains many veins and arteries that are connected to the central nervous system. Both subarachnoid space and subdural space are filled with cerebrospinal fluid (CSF).

2.3.2 The Cerebrospinal Fluid (CSF)

For a normal adult, the total volume of CSF is about 135 ml ~ 150 ml. Most of the CSF is in the subarachnoid space around the brain and in the spinal cord. A little amount of CSF fills in the cisterns around the brain. CSF protects the brain during an impact by diffusing a concentrated load more uniformly to the whole brain. CSF also protects nerves in the subarachnoid space and blood vessels in the subdural space from mechanical shock. CSF is also found in the ventricles located within the two halves of the cerebral hemisphere. There is a large fluid-filled space that lies behind the medulla oblongata and beneath the cerebellum. CSF carries nutrients to the brain. These fluid spaces are all interconnected with each other. For a normal adult, production of CSF is approximately 500 ml each day, and about 150 ml of CSF constantly circulates through and around the brain.

CSF is a colorless, slightly alkaline liquid composed of 99% water. It also contains a little lipid and proteins but no red blood cells. CSF can be regarded as an inviscid fluid similar to water. The tensile strength of CSF is approximately equal to that of water. CSF has the role of damping and cushioning for the brain [14].

2.4 The Vasculature and Axon Systems

A large amount of blood vessels and nerves embeds in and intertwine through the brain tissue. Rupture of vasculature and axons due to impacts is a major concern in studying brain injuries. However, mechanical responses of vasculature and axons to impacts are difficult to measure using current experiment technologies. Although numerical studies [52] have demonstrated that inclusion of vasculature in a finite element model does not considerably affect the macroscopic dynamic responses of brain tissue to impacts, it is more important to know how vasculature and axons behave under mechanical impacts.

2.4.1 The Vasculature System

Blood vessels spread over the surface of the cerebral hemispheres and within the subarachnoid space. Larger blood vessels generate smaller branch vessels that become more and more tiny. Types and distribution of blood vessels are different in different regions of the brain tissue. For example, there are more arterials deeper in the brain. For example, in the diencephalon, there mainly exist the internal carotid arteries and the proximal portions of the cerebral arteries. In contrast, the blood vessels on the superficial part of the brain, for example the gray matter of the cerebral cortex and the white matter, are branches of more distal portions of the vessel system. The density of blood is approx-

imately the same as CSF. A blood vessel consists of three concentric layers as shown in Figure 7. Blood vessels can be described as an elastomer, or neo-hookean material under quasi-static conditions [14]. Lots of experiments have been done to investigate the mechanical properties of vessels.

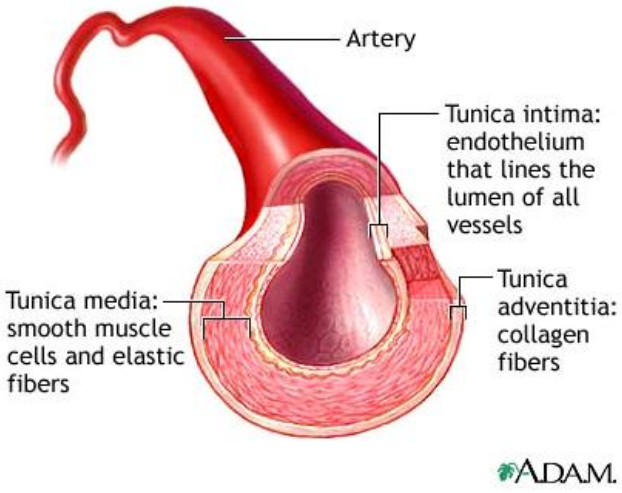

Figure 7 Anatomical structure of artery [53]

In experiments, blood vessels were stretched to failure in the longitudinal direction. It was demonstrated that axial stretching is the dominant deformation mode of the blood vessels. Arteries are considerably stiffer than the veins, carrying approximately twice as much stress at failure [54]. In the experiments conducted on vessels extracted from living human during epilepsy operations [55, 56], the cerebral vessel samples were stretched to failure in the longitudinal direction. The results of experiment samples are plotted in Figure 9, which provide persuasive data on the rupture limits of vessels. It should be noted

that the ultimate stresses of blood vessels are much lower than those of the skull and the brain tissues.

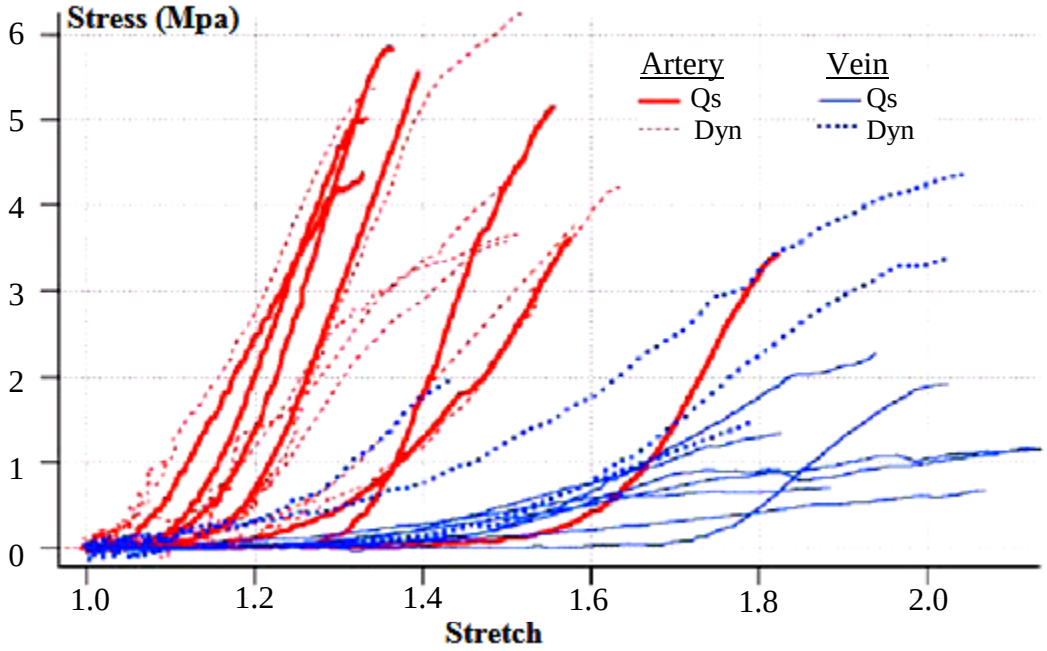

Figure 8 Quasi-static stress-strain curves for typical arteries and veins of cerebral vessels [56]

2.4.2 The Axon System

Another structure which is easy to be damaged in head injuries is axon system. Head injuries due to damage of axon system occur very frequently. For example, Diffuse Axons Injury (DAI) is one of the most severe head injuries. The axon system is the most complicated and the most highly organized system in the brain. Axon sizes are much smaller

than blood vessels. To study head injuries due to damage of axon system, strains or stresses in the brain tissue other than in axon and nerves are measured [57, 5].

Chapter 3

Finite Element Model of Human Head under Impacts

The following four factors affecting brain injuries were investigated using finite element modeling:

1) Cerebrospinal fluid
2) Cranium elasticity modulus
3) Impact contact area
4) Impact duration

Although it is possible to construct a three-dimensional finite element model for the problem, the objective of this thesis is to qualitatively investigate the effects of the above factors. Therefore, a two-dimensional finite element model is adequate for the research. The two-dimensional model represents a horizontal cross section of the human head as shown in Figure 9 (a). The two-dimensional model mainly includes the skull, the CSF, and brain

tissue (white matter, gray matter and corpus callosum). Geometric information of the head and intracranial anatomical structure required for constructing the two-dimensional model were extracted from magnetic resonance image, see Figure 9 (b). In this section, how the finite element model was constructed is described, which include the following steps:

1) Introduce assumptions
2) Construct geometric model
3) Describe material properties
4) Establish governing equations
5) Generate finite element mesh
6) Establish finite element equations

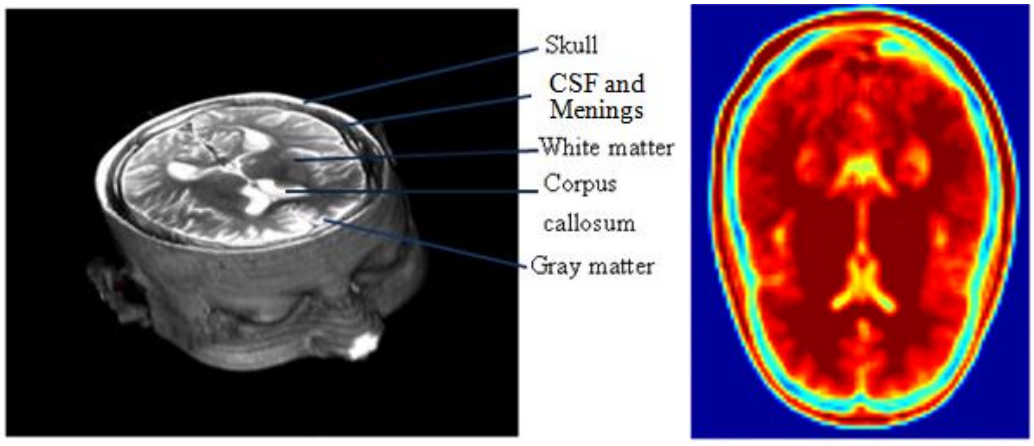

(a) (b)

Figure 9 (a) Anatomical structure of human head [58]; (b) Magnetic resonance image

3.1 Assumptions

To simplify the problem, a number of assumptions were introduced in developing the finite element model.

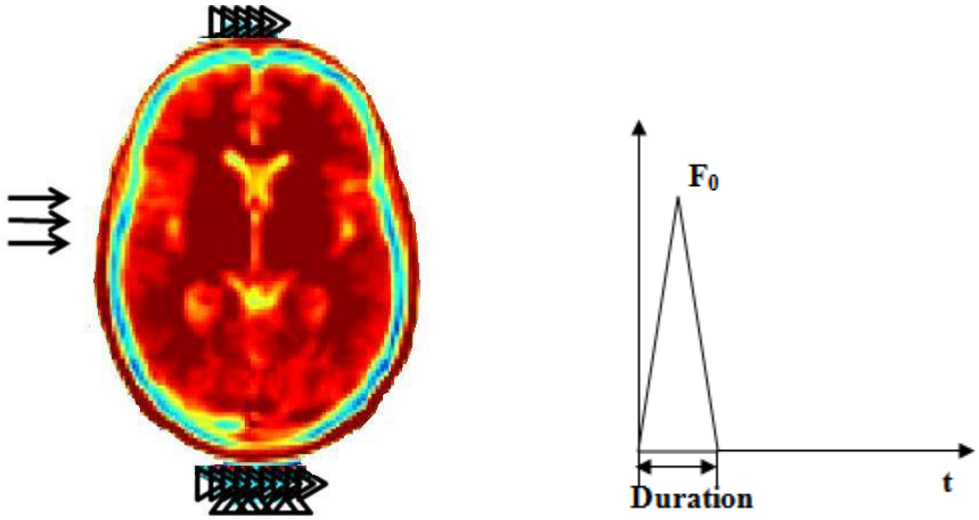

(a) (b)

Figure 10 (a) Locations of impact and constraint; (b) Triangular impact

- In a real-world head injury scenario, the head may have rigid-body motions under an impact. In this thesis it was assumed that no rigid-body motion is allowed so that a linear finite element model based on small displacements can be used. It was further assumed that the maximum peak stresses in the skull induced by impact are smaller than the material strength, so that no fracture would occur in the skull and the head injury can be considered as a closed head injury. The locations

of the impact and the constraints are shown in Figure 10(a). The impact is represented by a triangular impulse as shown in Figure 10(b).

- The intracranial anatomical structure of the human head is very complex. It is very difficult and unnecessary to consider all the anatomical details such as meninges, blood vessels and axons in this stage of the research. Therefore, the two-dimensional model was represented by three parts: the skull, the CSF, and the brain. The three parts represent the fundamental characteristics of the head. The skull is a very stiff solid material, CSF is a fluid, and the brain is soft visco-elastic material.
- As discussed in Chapter 2 on the anatomical structures of the head, the materials of the head are heterogeneous, anisotropic and nonlinear. In this thesis, simplified material models were introduced to describe the behaviour of the components of the head. The material of the skull was assumed elastic, isotropic and homogeneous. The material of the brain was assumed viscoelastic, isotropic, and homogeneous. It is generally agreed that cerebrum tissues are viscoelastic. As confirmed by in vivo experiments conducted on the brains of rats and monkeys, the stress-strain behaviour of cerebrum tissues is typically viscoelastic. It was also assumed that the convective and viscous effects of CSF can be omitted. The velocities of

CSF relative to the skull and the brain are very small and therefore negligible. The viscous effects by which deviatoric stresses are introduced can also be neglected [14].

3.2 Geometric Model

In the finite element model, the problem domain is defined by a geometric model. The geometric model is used to generate a finite element mesh. For the two-dimensional human head, the geometric model was constructed from magnetic resonance image. The key step in constructing the geometric model is to separate the skull, the CSF and the brain by identifying the boundaries between them.

3.2.1 Information captured by magnetic resonance imaging

In a magnetic resonance (MR) image, see Figure 9(b), the different color or pixel represents tissues having different content of protons. The basic principle of MR imaging is briefly described in the following. Different tissue in the human body contains different content of water. Each water molecule has two hydrogen nuclei or protons. Each proton has a positive pole and a negative pole. Protons are spinning. Spinning protons are little magnets. When placed in a strong magnetic field, these magnets (protons) will align with

the external magnetic field. In this process, protons will absorb some energy and oscillate at a frequency proportional to that field. When the field is turned off, protons of different tissues release energy with characteristic longitudinal and transverse relaxation times. These singles can be detected and amplified by the additional magnetic fields and used to construct the image. These signals produce different color or gray scale on the image. MRI is especially powerful for showing detailed inner geometrical information of the brain. MRI is a non-invasive imaging technique, which can be safely operated on living people. MRI provides much greater contrast between the different soft tissues of the body than other medical imaging modalities.

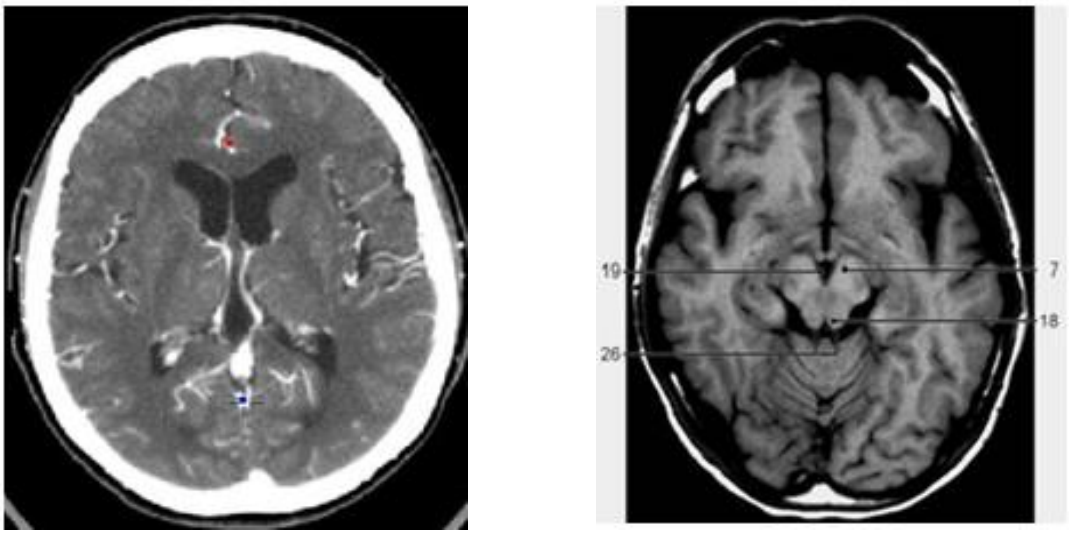

(a) (b)

Figure 11 (a) Computer Tomography (CT) scan; (b) Magnetic resonance image [4]

In Figure 11, a computed tomography (CT) scan and an MR image are shown. The MR image shows much greater contrast between the different brain tissues. Thus more accurate geometrical boundaries of different tissues can be extracted from an MRI image.

3.2.2 Segmentation of the three parts in human head

The skull, the CSF and the brain tissue need be segmented to construct the finite element model. Edge based segmentation method was used. MATLAB codes were written to extract boundaries between the three parts. Figure 12 shows the flow chart of the segmentation procedure.

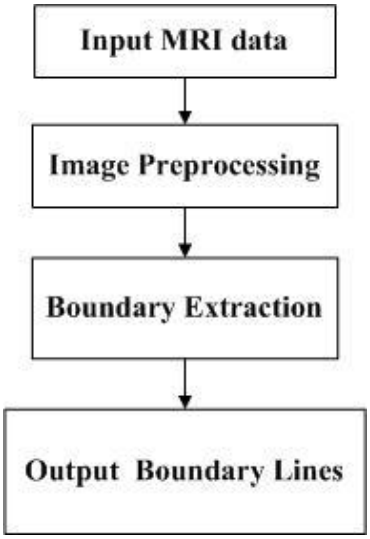

Figure 12 Flow chart of segmentation procedure

1. Input MRI data

Magnetic resonance image (MRI) data are stored as DICOM files which can be read into MATLAB directly using the ‘dicomread’ function. The loaded MR scan is a 256-by-256 array (resolution-dependent). The loaded MR image is plotted in MATLAB and shown in Figure 13.

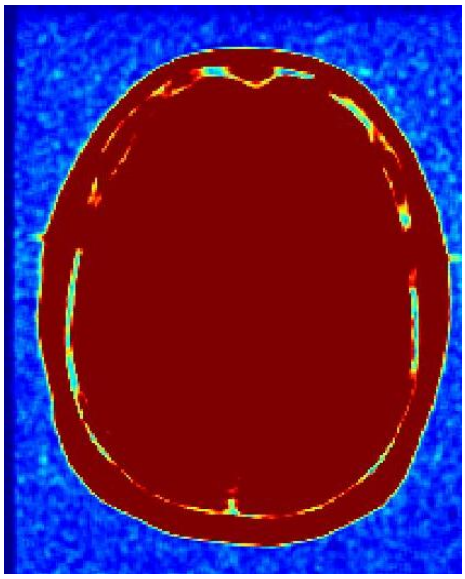

Figure 13 An MR image displayed in MATLAB

2. Image Processing

Image processing consists of two steps: contrast enhancement and noise filtering. The MATLAB function ‘imagesc’ is applied to enhance the contrast of pixel intensities. The function can scale original image data to the full range of the current color map. Part of the resulting image is displayed in Figure 14 (a), where different tissues have greater contrast. The boundaries are still blurring and outliers exist in many regions.

The image contains a number of uncertain spots which were induced due to the inherent technical limitations of the MRI technique, including random image noise, spectral leakage, MR signal intensity variation, non-uniform radiofrequency fields, etc [59].

The MATLAB function ‘smooth’ was adopted as a filter, which is a low pass filter with filter coefficients equal to the reciprocal of the span. The part of smoothed MR image is plotted in Figure 14(b). In the smoothed MR image, more clear iso-lines can be identified. These iso-lines were used to segment the three major parts of the head.

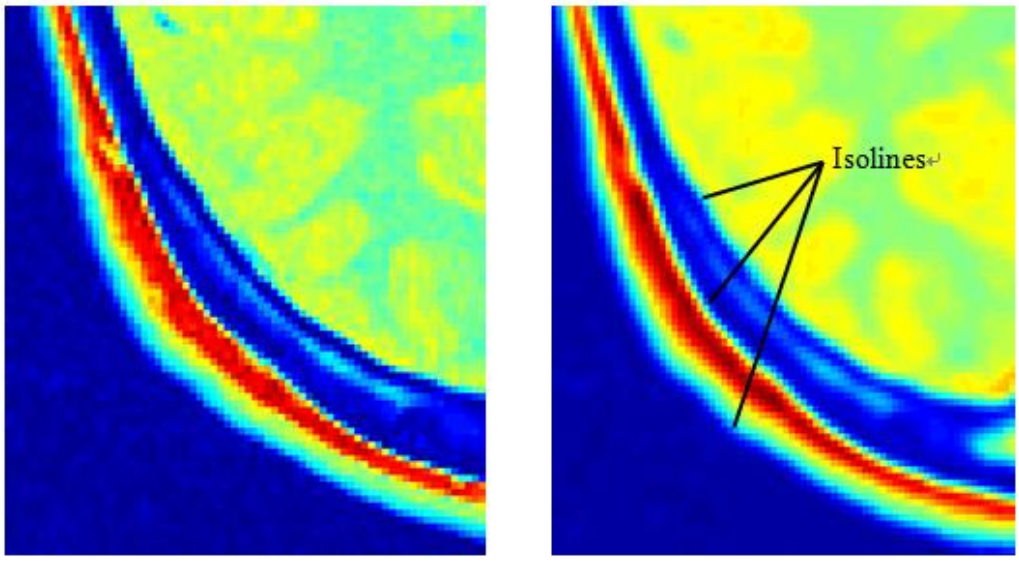

(a) (b)

Figure 14 (a) Enhanced MR image; (b) Smoothed MR image

3. Boundary Extraction

Light blue isolines were selected as the boundaries of the skull, the CSF, the brain and the background. To extract the isolines, MATLAB function ‘Contour’ was used. The MATLAB contour plot is able to calculate and display isolines based on color or gray scale in an image, see Figure 15(a). The light blue contour lines were picked up manually and the boundaries of three parts were obtained, see Figure 15(b). It must be pointed out that in an MR image, the boundary between fluid and soft tissue is vague. A different threshold may produce a slightly different geometric model. There are many light blue isolines in Figure 15(a), representing many different parts of tissue. For this reason, although an automatic segmentation procedure is possible, manual operation is much simpler for constructing the simple model in Figure 15(b).

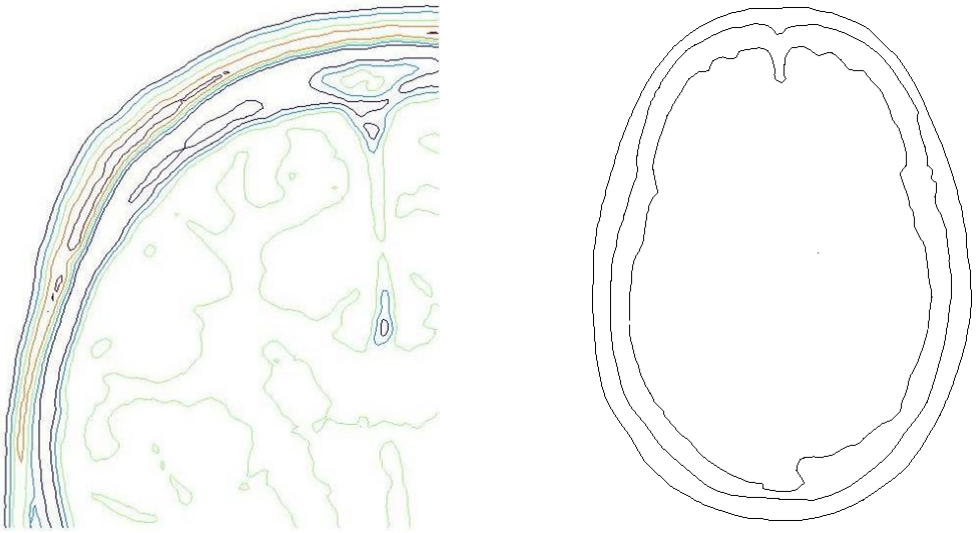

(a) (b)

Figure 15 (a) Isolines in MR image obtained by MATLAB contour function; (b) Boundaries extracted from the MR image

4. Output Boundary Lines

The boundaries were output as three line loops. The line loops were then input to ANSYS. The geometry of the two-dimensional head model was obtained from the areas (enclosed by the three line loops) by using ANSYS Boolean operators, see Figure 16.

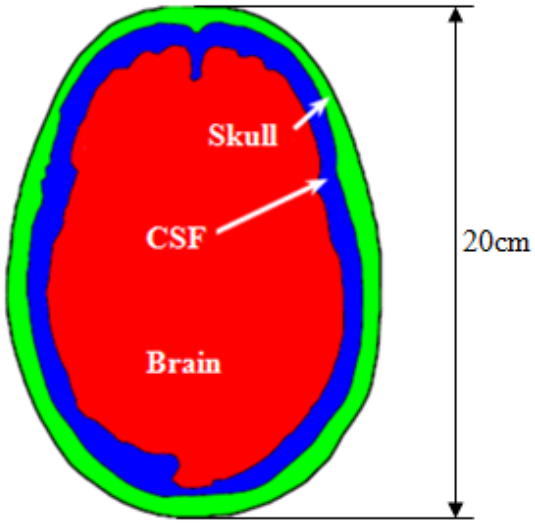

Figure 16 2D head model constructed by ANSYS

3.3 Material properties

The reported material properties for the three head parts are quite diverse because of the differences in test conditions, experiment methods and donor samples. In this study, the material parameters were extracted from [28, 60, 31] and they are listed in Table 2.

Table 2 Material properties of each component [28, 60, 31]

Material	Young's modulus (MPa)	Density (kg/m^3)	Poisson's ratio	Damp coefficient
Skull	6650	2080	0.22	
Brain	0.558	1040	0.45	0.009
CSF	1451.13	1040	0.499	

Based on the provided material properties, the average velocity of sound wave in the human head is approximately 1500 m/s. The characteristic width of a normal human head is about 0.2 m. Therefore, the time for a mechanical wave to travel across the head is about 0.1 ms.

3.4 Governing Equations

Based on the assumptions made in Section 3.1, governing equations of the two-dimensional head model under impact are provided in the following. As the rigid-body motions of the model are constrained, wave propagation will be the dominant response [61]. Mechanical wave generated by the impact will travel through the medium consisting of the stiff skull, the CSF, and the soft brain tissue. For the heterogeneity of the media, the following wave propagation phenomena will happen at the skull-CSF interface and the CSF-brain interface: 1) wave reflection; 2) wave refraction; 3) interference of incident

and reflected waves. The governing equations are the base for establishing finite element equations.

3.4.1 The Skull

For a tiny body isolated from the elastic solid medium, if body forces are ignored, its motions under the effect of a mechanical wave are governed by [62]:

$$\begin{cases} \dfrac{\partial \sigma_x}{\partial x} + \dfrac{\partial \tau_{xy}}{\partial_y} = \rho_s \ddot{u}_x \\ \dfrac{\partial \sigma_y}{\partial y} + \dfrac{\partial \tau_{xy}}{\partial_x} = \rho_s \ddot{u}_y \end{cases} \tag{3.1}$$

Where ρ_s is the mass density of the solid material; σ_x and σ_y are the normal stresses in x and y direction, respectively; τ_{xy} is the shear stress; u_x and u_y are the displacement in x and y direction; superposed dots denote the material time derivatives.

The equilibrium can also be represented in compact form as:

$$\nabla \cdot \boldsymbol{\sigma} = \rho_s \ddot{\mathbf{u}} \tag{3.2}$$

Where ∇ is the differential operator defined as $\nabla = \begin{bmatrix} \dfrac{\partial}{\partial x} & 0 & \dfrac{\partial}{\partial y} \\ 0 & \dfrac{\partial}{\partial y} & \dfrac{\partial}{\partial x} \end{bmatrix}$;

$\boldsymbol{\sigma}$ is the stress vector defined as $\boldsymbol{\sigma} = \begin{Bmatrix} \sigma_x \\ \sigma_y \\ \tau_{xy} \end{Bmatrix}$; and the displacement vector defined as $\mathbf{u} = \begin{Bmatrix} u_x \\ u_y \end{Bmatrix}$.

3.4.2 The Brain Tissues

Differential governing equations for the viscoelastic brain tissues are given by:

$$\begin{cases} \dfrac{\partial \sigma_x}{\partial x} + \dfrac{\partial \tau_{xy}}{\partial_y} + \mu_x \dot{u}_x = \rho_s \ddot{u}_x \\ \dfrac{\partial \sigma_y}{\partial y} + \dfrac{\partial \tau_{xy}}{\partial_x} + \mu_y \dot{u}_y = \rho_s \ddot{u}_y \end{cases} \tag{3.3}$$

where μ_x and μ_y are viscosity parameters describing the material damping property.

The equilibrium can also be represented in the form as [62]:

$$\nabla \cdot \boldsymbol{\sigma} + \boldsymbol{\mu} \dot{\mathbf{u}} = \rho_s \ddot{\mathbf{u}}, \tag{3.4}$$

where ∇ , $\boldsymbol{\sigma}$ and $\mathbf{u}$ have the same meanings as in Equation (3.2). $\boldsymbol{\mu} = \begin{bmatrix} \mu_x & 0 \\ 0 & \mu_y \end{bmatrix}$.

3.4.3 The CSF

Wave propagation in a two-dimensional liquid medium is governed by a second order partial differential equation given as follows [63]:

$$\frac{1}{c^2} \frac{\partial^2 p}{\partial t^2} - \nabla^2 p = 0, \tag{3.5}$$

where c is the speed of sound in the fluid medium and $c=\sqrt{k/\rho_0}$; k is the bulk modulus of the fluid, and ρ_0 is the mean fluid density, or static density; p is the acoustic pressure; and t is the time variable; ∇^2 is the Laplace operator and given by: $\nabla^2 = \frac{\partial^2}{\partial x^2} + \frac{\partial^2}{\partial y^2}$.

3.4.4 Interaction between CSF and Solids

There are two interfaces in the biomechanical model that are shared by two different media: the skull-CSF interface and the CSF-brain interface. At a fluid-solid interface, the governing equation is established by considering the interaction between the normal pressure gradient of the fluid and the normal inertia force of the solid:

$$n^T \cdot \nabla p = -n^T \cdot (\rho_0 \ddot{u}), \tag{3.6}$$

where n is the normal of fluid-solid interface pointing to the fluid region, p is the acoustic pressure; and t is the time variable; ∇ is differentiation operator and given by: $\nabla = \left[\frac{\partial}{\partial x} \quad \frac{\partial}{\partial y}\right]$.

3.5 Finite Element Mesh

One step in establishing a finite element model for the human head under impact is to generate a finite element mesh. Both mesh density and mesh quality have significant effects on the accuracy of finite element solutions. The density of a finite element mesh is

defined as the number of elements in a unit area or unit volume of the problem domain. Mesh quality is mainly related to the shapes of finite elements. The geometric model constructed in Section 3.2 and shown in Figure 16 was used to generate the finite element mesh, so that the geometry represented by the finite element mesh is faithful to the head. The free mesh function of ANSYS was used to generate the mesh. The generated mesh consists of unstructured quadrilateral elements, see Figure 17. Quadrilateral elements are preferred as they produce higher solution accuracy compared to triangle elements if the same number of element nodes is used. In general, a finite element mesh should satisfy a number of requirements to achieve higher solution accuracy:

1. Smaller elements should be used in regions where finite element solutions may have larger variation or gradient.
2. The ratio of an element's longest edge to its shortest edge should be close to unit.
3. All interior angles of an element should be approximately equal.
4. Transition from larger elements to smaller ones should gradual.

However, some of the requirements are difficult to fulfil without using an automatic mesh adaptation algorithm. The finite element mesh shown in Figure 17 was used in the numerical investigations. In total, the mesh includes 3235 elements, 583 key points and 3372 nodes.

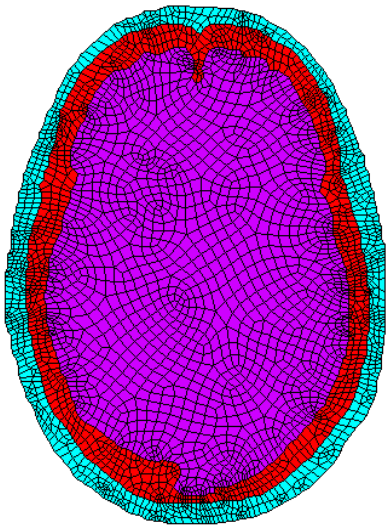

Figure 17 Finite element mesh used in numerical investigations

3.6 Finite Element Equations

By following the standard Galerkin procedure [63], finite element equations can be established from the governing equations given in Eqs. (3.2), (3.4), (3.5), and (3.6). The finite element equations for the skull are obtained as:

$$\left[\mathrm{M}^{\mathrm{S}}\right]\{\ddot{\mathbf{u}}\}+\left[\mathrm{K}^{\mathrm{S}}\right]\{\mathbf{u}\}=\{\mathbf{F}_{\mathbf{t}}\}, \tag{3.7}$$

Where $\left[\mathrm{M}^{\mathrm{S}}\right]$ is the mass matrix; It has the expression $\left[\mathrm{M}^{\mathrm{S}}\right]=\int_{\Omega_{\mathrm{S}}}\rho_{\mathrm{s}}\mathrm{N}_{\mathrm{u}}^{\mathrm{T}}\mathrm{N}_{\mathrm{u}}\mathrm{d}\Omega$; $\left[\mathrm{K}^{\mathrm{S}}\right]$ is the stiffness matrix and defined as $\left[K^{S}\right]=\int_{\Omega S}B_{u}^{T}\mathrm{D}B_{u}d\Omega$; $\{\mathbf{F}_{\mathbf{t}}\}$ represents the load vector resulted from the applied impact. $\mathrm{N_u}$ contains element shape functions for displacements; and $\left[\mathrm{B}_{\mathbf{u}}\right]=\{\mathrm{L}\}\{\mathrm{N}_{\mathbf{u}}\}^{\mathrm{T}}$ is the *B*-matrix obtained by operating the shape functions with the differentiation operator $\{\mathrm{L}\}$.

For viscoelastic brain tissue, finite element equations are obtained as:

$$[M^S]\{\ddot{\mathbf{u}}\}+[C^S]\{\dot{\mathbf{u}}\}+[K^S]\{\mathbf{u}\}=\mathbf{0}, \tag{3.8}$$

where $[C^S]$ is the damping matrix of viscoelastic brain tissue; it is defined as $[C^S]=\int_{\Omega_S} N_u^T \boldsymbol{\mu} N_u d\Omega$.

To obtain finite element equations for CSF, Eq. (3.5) is multiplied by a virtual change in pressure and integrating over the domain occupied by CSF. After combining Eq. (3.6), the variation expression is obtained as [64, 65]:

$$\int_{\Omega_F}\frac{1}{c^2}\delta P\frac{\partial^2 P}{\partial t^2}d\Omega_F+\int_{\Omega_F}\left(\{L\}^T\delta P\right)\left(\{L\}P\right)d(\Omega_F)=-\int_S\rho_0\delta P\{n\}^T\left(\frac{\partial^2}{\partial t^2}\{\mathbf{u}\}\right)d(S), \tag{3.9}$$

By introducing shape functions and conducting integration by parts, Eq.(3.9) can be transformed into the following form [63]:

$$[M^f]\{\ddot{\mathbf{p}}\}+[K^f]\{\mathbf{p}\}+[C^f]\{\dot{\mathbf{p}}\}+\rho_0[R_e]^T\{\mathbf{u}\}=\{\mathbf{0}\}, \tag{3.10}$$

Where $[M^f]=\frac{1}{c^2}\int_{\Omega_F}\{N_f\}\{N_f{}^T\}d\Omega$ is the fluid mass matrix; $[K^f]=\int_{\Omega_F}\{B_f{}^T\}\{B_f\}d\Omega$ is the fluid stiffness matrix; $\rho_0[R_f]=\rho_0\int_S\{N_f\}\{n\}\{N_u\}^T dS$ is the coupling matrix yielded from fluid-structure interaction; $[C^f]=\frac{\beta}{c}\int_{\Omega_f}\{N_f\}\{N_f\}^T d\Omega_f$ represents the fluid damping matrix; and β is the boundary absorption coefficient.

By introducing the fluid-solid interaction term into Eqs. (3.7) and (3.8), and then combining the two equations together, the following equation was obtained [63]:

$$[M^s]\{\ddot{\mathbf{u}}\}+[C^s]\{\dot{\mathbf{u}}\}+[K^s]\{\mathbf{u}\}-[\mathrm{R}^s]\{\mathbf{p}\}=\{\mathbf{F_t}\}, \tag{3.11}$$

The finite element equations in Eqs.(3.10) and (3.11) can be further combined into the following equation:

$$\begin{bmatrix} M^S & 0 \\ M^{fS} & M^f \end{bmatrix}\begin{Bmatrix}\ddot{\mathbf{u}}\\ \ddot{\mathbf{p}}\end{Bmatrix}+\begin{bmatrix} C^S & 0 \\ 0 & C^f \end{bmatrix}\begin{Bmatrix}\dot{\mathbf{u}}\\ \dot{\mathbf{p}}\end{Bmatrix}+\begin{bmatrix} K^S & K^{Sf} \\ 0 & K^f \end{bmatrix}\begin{Bmatrix}\mathbf{u}\\ \mathbf{p}\end{Bmatrix}=\begin{Bmatrix}\mathbf{F_t}\\ \mathbf{0}\end{Bmatrix}, \tag{3.12}$$

The matrices in the above equation have the following expressions:

$$M^s=\int_{\Omega_s}\rho_s N_u^T N_u d\Omega;\quad M^f=\frac{1}{c^2}\int_{\Omega_s}\rho_s N_u^T N_u d\Omega;\quad M^{fs}=\rho_0\int_s \rho_s N_p^T n^T N_u dS;\quad C^s=\int_{\Omega_S} N_u^T u\ N_u d\Omega;$$

$$C^f=\frac{1}{c}\int_s N_p^T u\ N_p dS;\quad K^s=\int_{\Omega_S} B_u^T D B_s d\Omega;\quad K^f=\int_{\Omega_f} B_p^T B_p d\Omega;\quad K^{sf}=-\int_s N_u^T n N_P dS,$$

where D is the material property matrix for the solid parts. Ω_s and Ω_f are the sub-domains occupied by the solids and the fluid, respectively. *S* represents the interface surface between the solid parts and the fluid.

Chapter 4

Numerical Investigations and Results

Based on the finite element model constructed in Chapter 3, numerical investigations were conducted to study the role of CSF in protecting the brain, the effects of cranium elasticity modulus, impact contact area, and impact duration on closed head injuries [66, 67]. To quantitatively evaluate the effects, the following mechanical responses were monitored in the investigations:

(b) First principal strain in the brain;

(c) von Misses strain in the brain;

(d) First principal stress in the skull;

(e) von Misses stress in the skull.

The maximum peak values of the above quantities are believed directly related to head injuries. The brain tissue is a viscoelastic material. Its damage is mainly characterized by maximum strains, especially maximum tensile strains. The skull behaves more like a linear elastic material. Its failure is mainly governed by maximum stresses.

4.1 The role of CSF in protecting the brain

To study the role of CSF in protecting the brain, two finite element models were studied and compared. The two models are shown in Figure 18. The only difference between them is that in one model, CSF is treated as a fluid; in the other, CSF is considered as a solid material having very low elasticity modulus. The other conditions were kept the same for the two models. The impact magnitude was set to $F_0 = 8000N$, and impact duration was changed in the scope of 0.1 ms ~ 1.0 ms, see Figure 10(b).

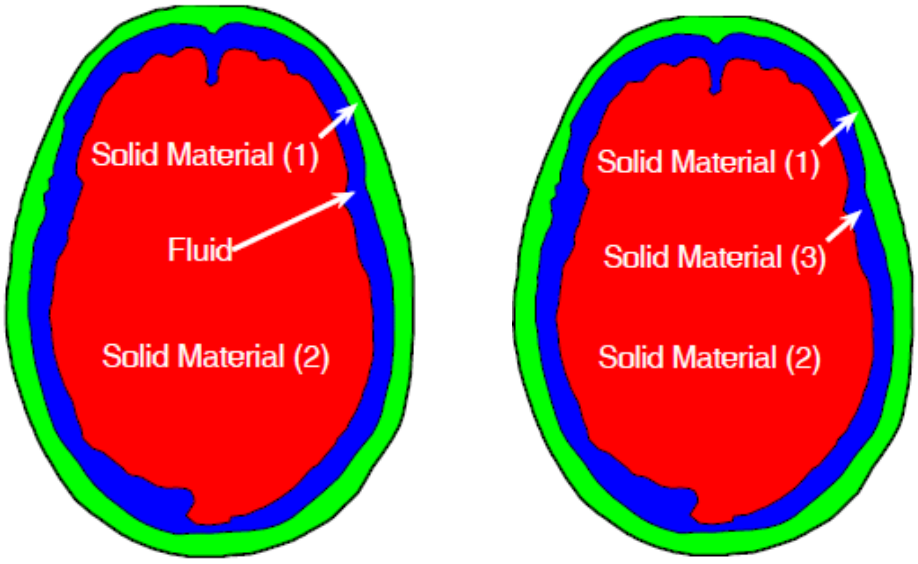

(a) (b)

Figure 18 (a) Model with CSF; (b) Model without CSF

The obtained results are plotted in Figure 19. It can be observed that the maximum peak values of the first principal strains and the von Misses strains predicted by the model with CSF are consistently lower than those from the model without CSF. The results verify

that CSF does provide a natural protection to the brain. The CSF has the function of distributing a concentrated impact more uniformly to the whole brain. The maximum peak values of mechanical responses are thus reduced.

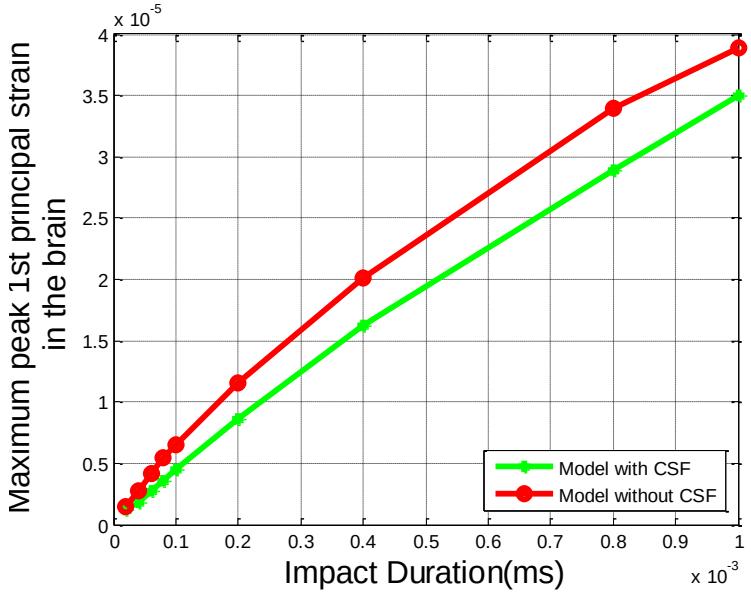

(a)

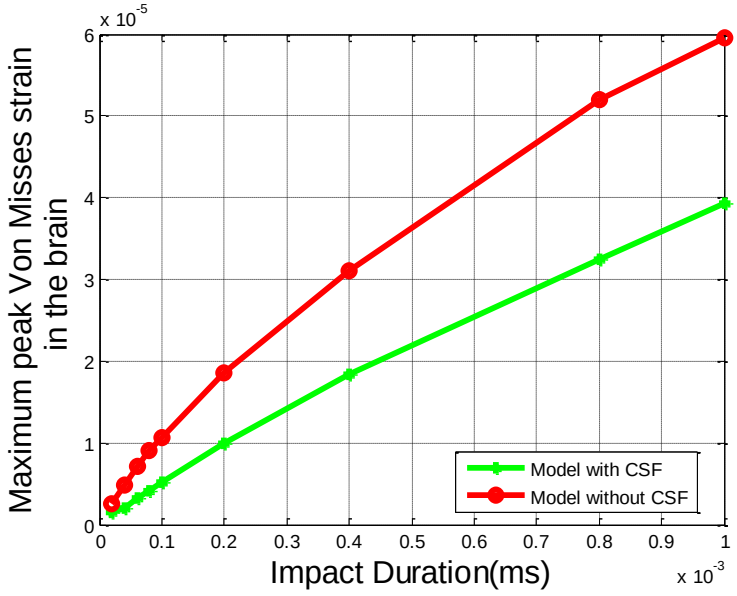

(b)

Figure 19 (a) Maximum peak 1st principal strain in the brain; (b) Maximum peak von Misses strain in the brain.

The relative differences between the two models are calculated in the following so that a quantitative measurement on the role of CSF can be obtained. The relative difference of a mechanical response is defined as:

$$\text{(Relative Difference)} = \frac{|\,(With \quad CSF) - (Without \quad CSF)\,|}{(With \quad CSF)}$$

The calculated relative differences are listed in Table 3 and 4.

Table 3 Relative difference in maximum peak first principal strain

Impact Duration (ms)	Max. 1st principal strain with CSF	Max. 1st principal strain without CSF	Relative Difference (%)
1.00	3.50e-5	3.80e-5	10.03
0.80	2.89e-5	3.40e-5	17.60
0.40	1.62e-5	2.01e-5	24.07
0.20	8.67e-6	1.15e-5	32.18
0.10	4.52e-6	6.46e-6	42.92
0.08	3.59e-6	5.43e-6	51.25
0.04	1.81e-6	2.80e-6	54.70

Table 4 Relative difference in maximum peak effective strain

Impact Duration (ms)	Max. peak effective strain with CSF	Max. peak effective strain without CSF	Relative Difference (%)
1.00	3.93e-5	5.95e-5	51.40
0.80	3.25e-5	5.20e-5	60.00
0.40	1.83e-5	3.11e-5	69.95
0.20	9.91e-6	1.85e-5	86.87
0.10	5.21e-6	1.07e-5	105.37
0.08	4.13e-6	9.06e-6	119.37
0.04	2.09e-6	4.77e-6	128.23

The following observations can be made from the above results:

1. The CSF does play a very important role in protecting human brain that cannot be ignored from biomechanical model used for in studying head injuries. The relative difference in the mechanical responses from the models with and without CSF can be as high as mechanical response in model without fluid component can be as much as 128.23%.
2. It can also be observed that the protection effectiveness is dependent on impact duration. For ballistic impacts that have very short durations (<0.1 ms), the protection role of CSF is more significant. With impact duration reduced from 1 ms to 0.04 ms, the relative differences between mechanical responses from the two models are considerably increased. This phenomenon is caused by the 'cushioning' property of fluid. A fluid has damping effect, even it is considered inviscid. The damping effect will become stronger if the impact has a shorter duration.
3. CSF has larger influence on von Misses strain compared with the first principal strain. This is because an inviscid fluid cannot withstand shear strain. Thus in the model with the CSF, the shear strains are filtered out by the CSF layer, and no shear strain is transferred from the skull to the brain during an impact.

4. The protection effect of CSF is related to its fluid characteristic. It seems that, to prevent dynamic energy transmitting into brain in closed head injuries, fluid material has more effective cushion than the solid material of similar material property parameters. Thus, better protection could be provided if the padding material of a helmet is made from a fluid-solid mixed material other than totally solid. This measure should increase the protection effectiveness of helmet, which deserves a further study.

The process of the generation and propagation of strain wave induced by the impact is shown in Figure 20. The following phenomena can be observed from the screen shots.

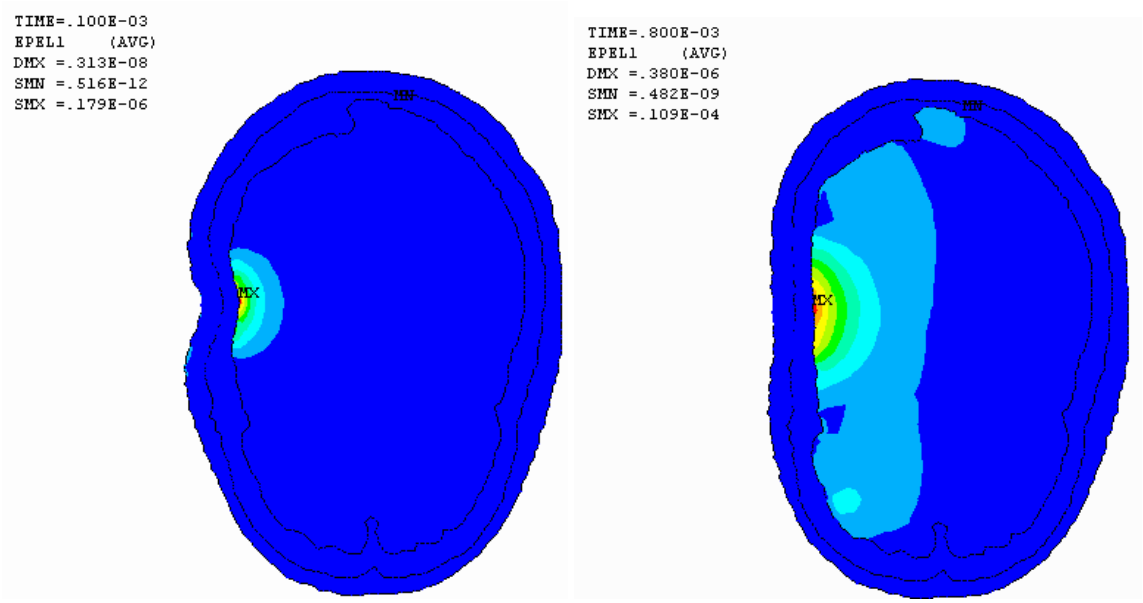

(a) t=0.1 ms (b) t=0.8 ms

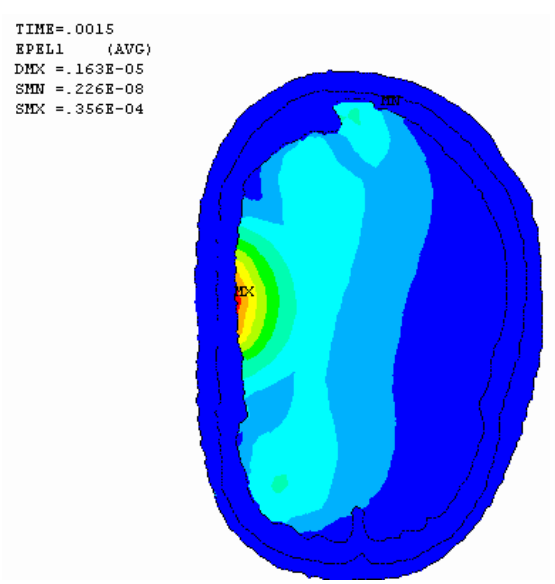

(c) t=1.5 ms

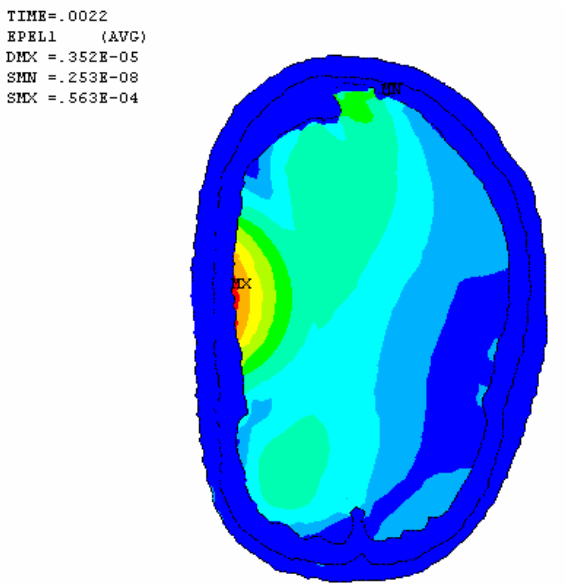

(d) t=2.2 ms

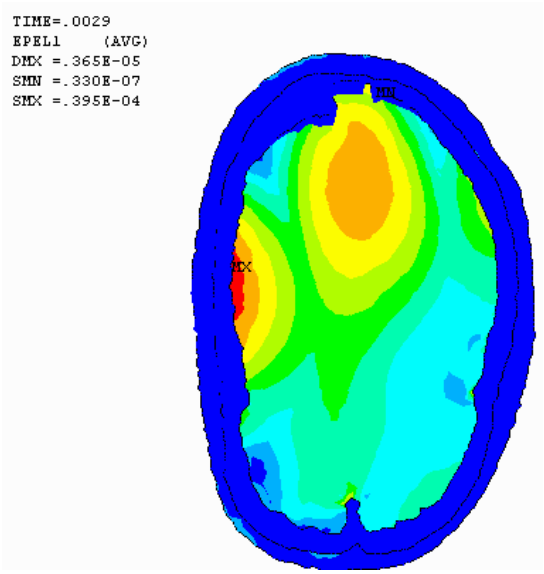

(e) t=2.9 ms

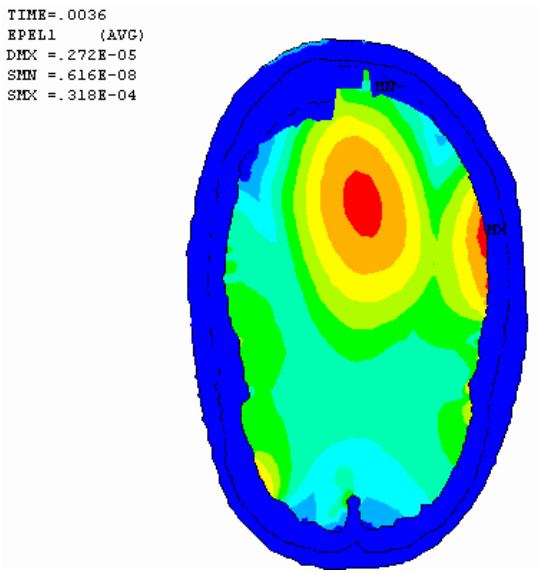

(f) t=3.6 ms

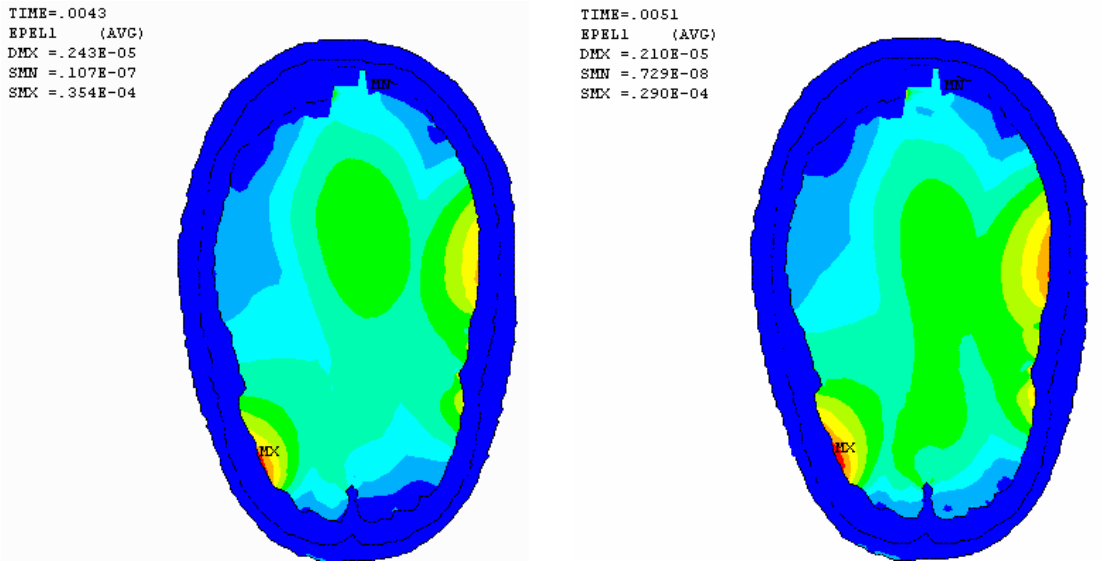

(g) t=4.3 ms (h) t=5.1 ms

Figure 20 Mechanical waves generated by impact and their propagation in the head

1) Maximum strains at different time instants can occur in the interior of the brain, or at CSF-brain interface. If a maximum strain exceeds the ultimate strain the brain tissue can sustain, a contusion would be caused by the strain.

2) In Figure 20(f), it can be seen that a maximum strain appeared on the side that is opposite to impact side. In the literature of head injuries, the side where an impact strikes is called the coup side and the side opposite to the impact side is called contrecoup side. In the so-called coup-contrecoup phenomenon, brain injuries may occur at both the coup side and the contrecoup side. The screen shots, see Figure 20 (e) and (f), show that coup-contrecoup phenomenon may occur if the

maximum strains occurred at the coup and the contrecoup side exceeds the ultimate strain of the brain tissue.

4.2 Effect of cranium elasticity modulus

Cranium elasticity modulus changes considerably with age. For a one-week infant, the elasticity modulus of the cranial bone is about 820.9MPa [44]. While for an adult, the average cranium elastic modulus is around 15.54GPa. Therefore, in our investigations on the effects of cranium elasticity modulus on closed head injuries, we selected a number of values from the range of 820.9MPa to 15.54GPa. In the finite element simulations other conditions were kept constant except cranium elasticity modulus and impact duration. The same impact magnitude and impact contact area used in Section 4.1 were used in this investigation. Impact durations of 0.2ms, 0.8ms, and 1.2ms were applied. The obtained simulation results are plotted in Figure 21.

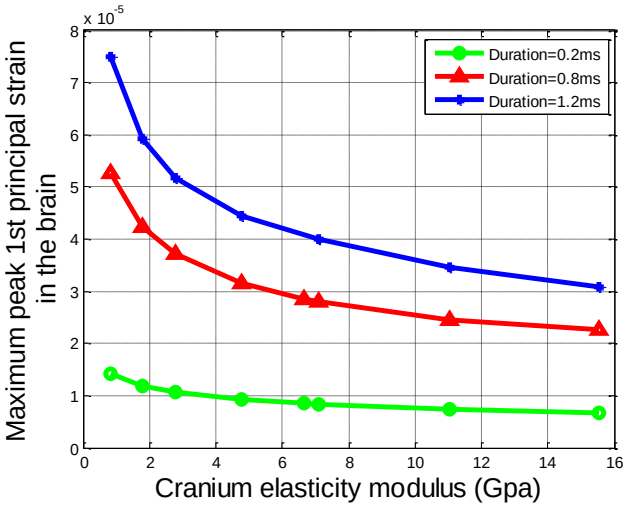
x 10^-5
Maximum peak 1st principal strain in the brain
Cranium elasticity modulus (Gpa)
Duration=0.2ms
Duration=0.8ms
Duration=1.2ms

(a)

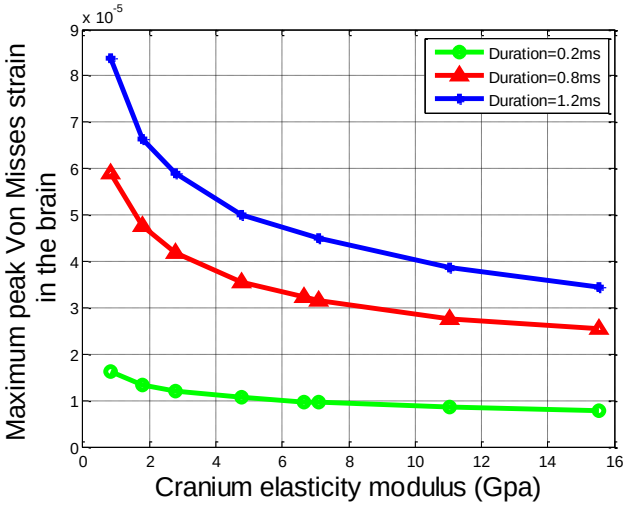
x 10^-5
Maximum peak Von Misses strain in the brain
Cranium elasticity modulus (Gpa)
Duration=0.2ms
Duration=0.8ms
Duration=1.2ms

(b)

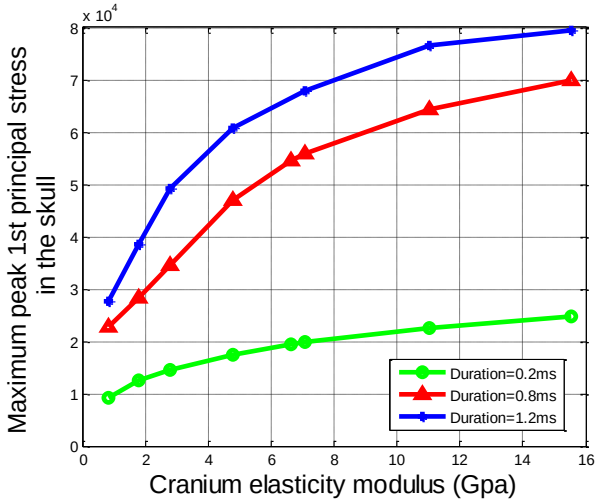
x 10^4
Maximum peak 1st principal stress in the skull
Cranium elasticity modulus (Gpa)
Duration=0.2ms
Duration=0.8ms
Duration=1.2ms

(c)

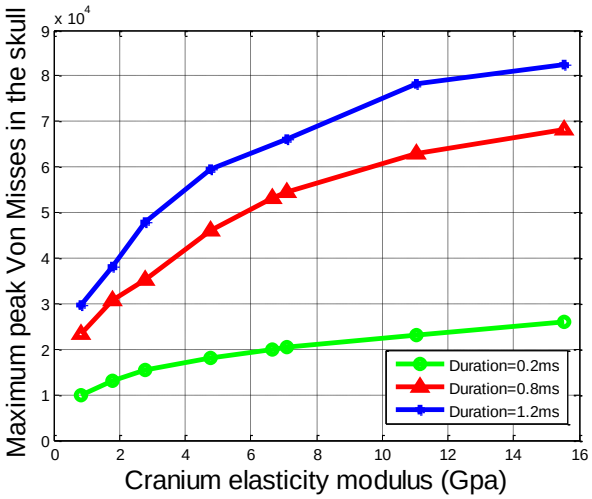

(d)

Figure 21 (a) Maximum peak 1st principal strain in the brain;
(b) Maximum peak von Misses strain in the brain;
(c) Maximum peak 1st principal stress in the skull;
(d) Maximum peak Von Misses stress in the skull

For a better understanding of the influence of cranium elasticity modulus, reduction percentages of peak strains in the brain are calculated and listed in Table 5. The reduction percentage is defined as:

$$(\text{Reduction Percentage}) = \frac{(\textbf{M}\text{aximum strain}) - (\textbf{M}\text{inimum strain})}{(\textbf{M}\text{aximum strain})}$$

Table 5 Reduction percentage of maximum peak strain in the brain

Impact Duration / **Mechanical Response in Brain**	0.2 ms	0.8 ms	1.2 ms
Reduction in maximum peak 1st principal strain	52.3%	53.3%	58.9%
Reduction in maximum peak von Misses strain	51.8%	53.1%	58.8%

The following observations can be made from the computational results:

1. Cranium elasticity modulus greatly affects the strain level in the brain. The brain would have smaller strains if the cranium stiffness is increased. The reduction percentage of maximum peak 1st principal strain and maximum peak von Misses strain are approximately the same. With cranium elasticity modulus increasing from 820.9MPa to 15.6GPa, maximum peak 1st principal strain and maximum peak von Mises strain were reduced by more than 50% for all the three impact durations.
2. It can be observed from the curves shown in Figure 21 that both the maximum peak 1st principal strains and the maximum von Mises strains in the brain decrease significantly as the cranium elasticity modulus increases from 820.9 MPa to 5 GPa. For the range of cranium elasticity modulus larger than 5 GPa, increases in cranium elasticity modulus have very little further effect on the maximum peak strains in the brain.
3. The maximum peak 1st principal stress and maximum peak von Mises stress in the skull are increased with increasing cranium elasticity modulus, see Figure 21 (c) and (d).

The above investigation results indicate that children are more vulnerable to head injuries and wearing a helmet can effectively reduce the chance and the severity of head injuries for kids. For children under the age of eight, cranium elasticity modulus is usually below 4GPa. Wearing a helmet has the effect to increase the elasticity modulus of the protection

layers. The investigation results also indicate that it is not necessary that the larger the stiffness, the better the helmet is. After reaching a certain level, the stiffness of helmet may have very little effect on strains in the brain, but the weight of the helmet may be increased. The optimal stiffness of a helmet need be determined by further study.

4.3 Effect of impact contact area

The objective of investigations reported in this section was to study the effect of impact contact area. The total impact force was kept as a constant (128 N). However, the contact area (i.e. contact length for two-dimensional model) was gradually increased from 0.9 cm to 10 cm. Three impact durations, 1 ms, 0.8 ms, and 0.2 ms, were studied. Other conditions were kept unchanged. Simulation results are plotted in Figure 22. Reduction percentages were calculated and listed in Table 7.

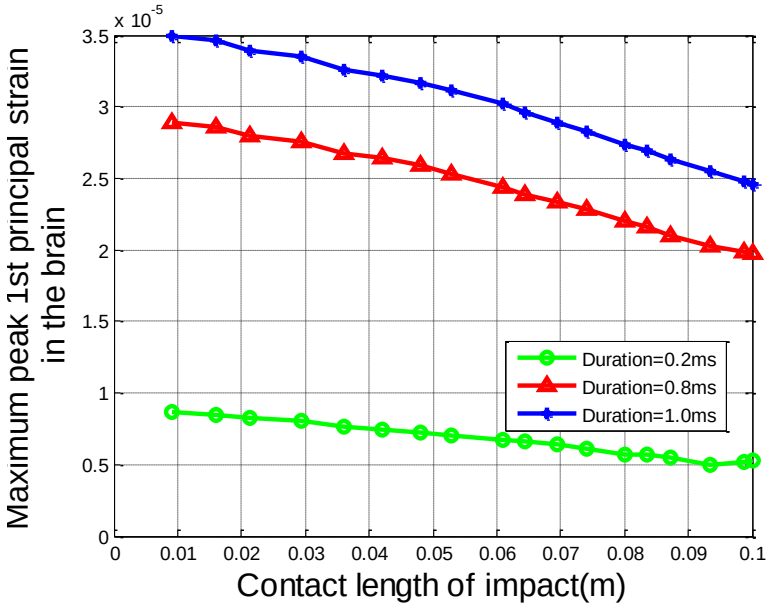
x 10^-5
Maximum peak 1st principal strain in the brain
Contact length of impact(m)
Duration=0.2ms
Duration=0.8ms
Duration=1.0ms

(a)

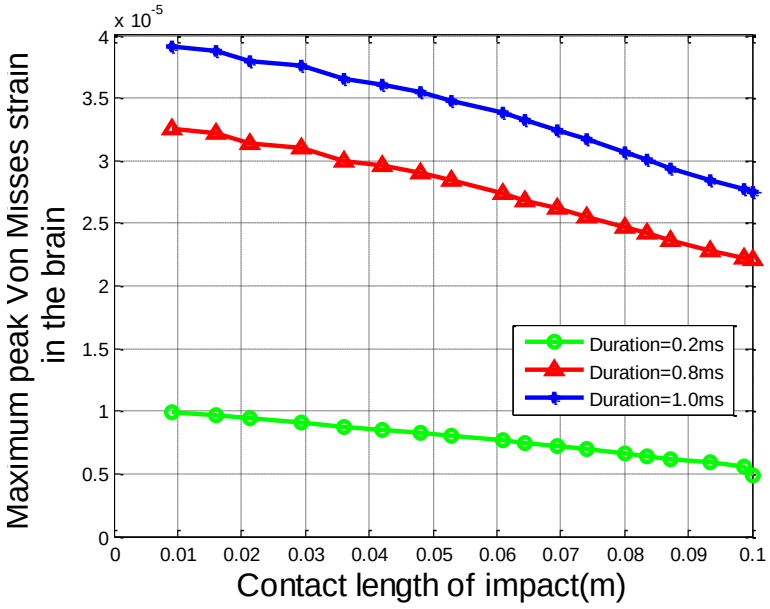
x 10^-5
Maximum peak Von Misses strain in the brain
Contact length of impact(m)
Duration=0.2ms
Duration=0.8ms
Duration=1.0ms

(b)

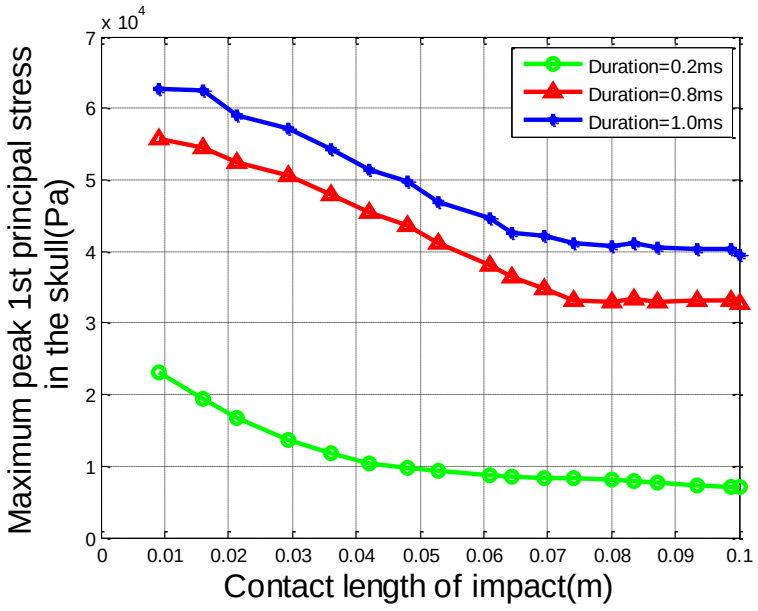

(c)

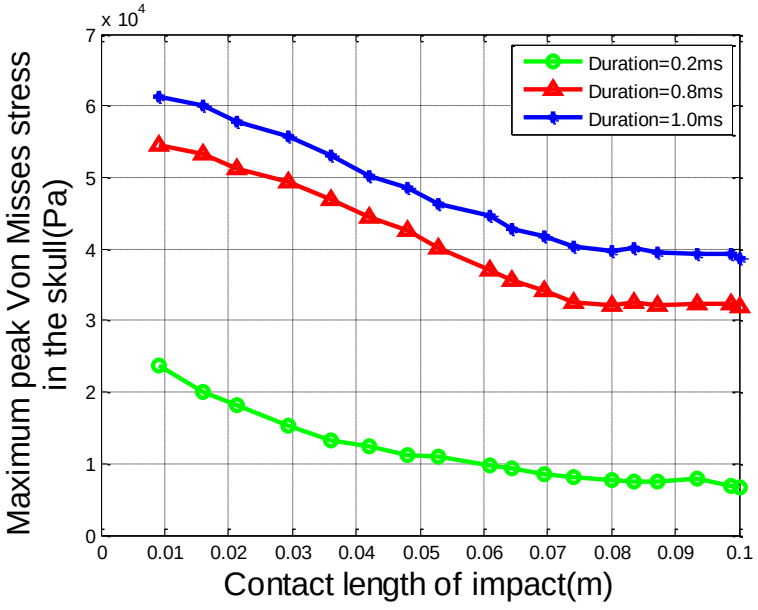

(d)

Figure 22 (a) Maximum peak 1st principal strain in the brain;
(b) Maximum peak von Misses strain in the brain;
(c) Maximum peak 1st principal stress in the skull;
(d) Maximum peak von Misses stress in the skull

Table 6 Reduction percentage of maximum peak strain and stress values

Mechanical Response \ Impact duration	0.2 ms	0.8 ms	1.0 ms
Maximum peak 1st principal strain in the brain	39.6%	31.5%	29.5%
Maximum peak Von Misses strain in the brain	40.7%	32.0%	29.7%
Maximum peak 1st principal stress in the skull	69.7%	41.2%	36.9%
Maximum peak von Misses principal stress in the skull	71.6%	41.3%	37.0%

The obtained results indicate that:

1. Increase of contact length leads to reduction of maximum peak strains in the brain. For example, for the impact duration of 0.8 ms, both the maximum peak 1st principal strain and the maximum peak von Misses strain decrease by about 30% with the impact contact area (length) increasing from 0.9 cm to 10 cm.
2. Increase of impact contact area also helps reducing stresses in the skull. Reduction of stresses in the skull by increasing contact area is more considerable for shorter impact durations. Maximum peak stresses in the skull are reduced by 35%-50% with contact area (length) increased from 0.9 cm to 7 cm. Reduction of stresses is slow down after the contact area (length) reaches 7 cm (less than half of the head height).

3. The effectiveness of reducing strains in the brain and stresses in the skull is related to impact duration. For shorter impact durations, the reduction is more remarkable. For example, the strains are reduced by about 40% for impact duration of 0.2 ms, compared to the reduction of about 30% for impact duration of 1.0 ms. The above observation is even more obvious for reductions of stresses in the skull, 71.6% under impact duration of 0.2 ms, and about 37% under impact duration 1.0 ms.

Increasing impact contact area is an effective method to reduce the strains in the brain and the stresses in the skull. A protective helmet has the functionality of increasing contact area between impact force and the skull, distributing the impact force to a larger area, and thus protecting the skull and the brain. Simulation results show that the effectiveness is related to impact duration. Further increase of contact area (length > 8 cm) does not help reducing the strains and the stresses.

4.4 Effect of impact duration

Effect of impact duration was investigated in the similar way as in the previous investigations. In the investigations, the total impulse, i.e. the area of the triangular impact shown in Figure 10(b), was kept as a constant; the duration of the impact was gradually increased. Other conditions were kept unchanged. Two impulse magnitudes, 0.45 Ns and

0.6 Ns, were applied. Simulation results are shown in Figure 23. Reduction percentage were calculated and listed in Table 7.

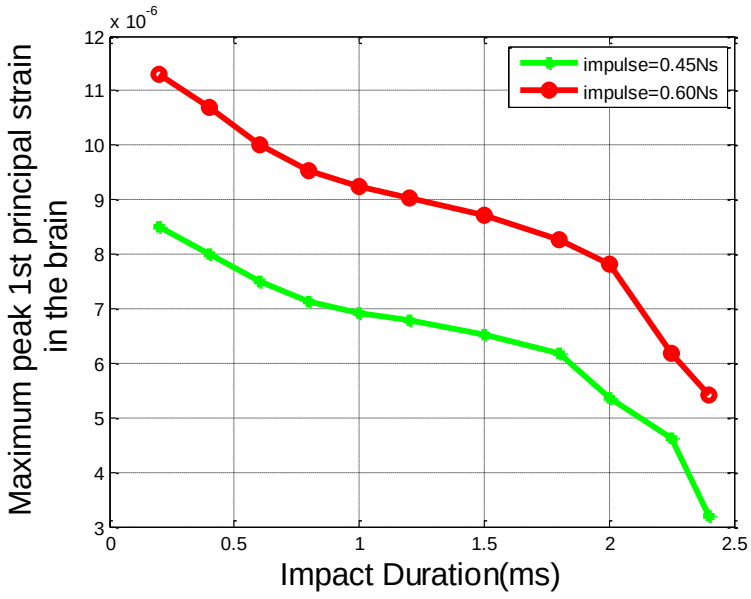

(a)

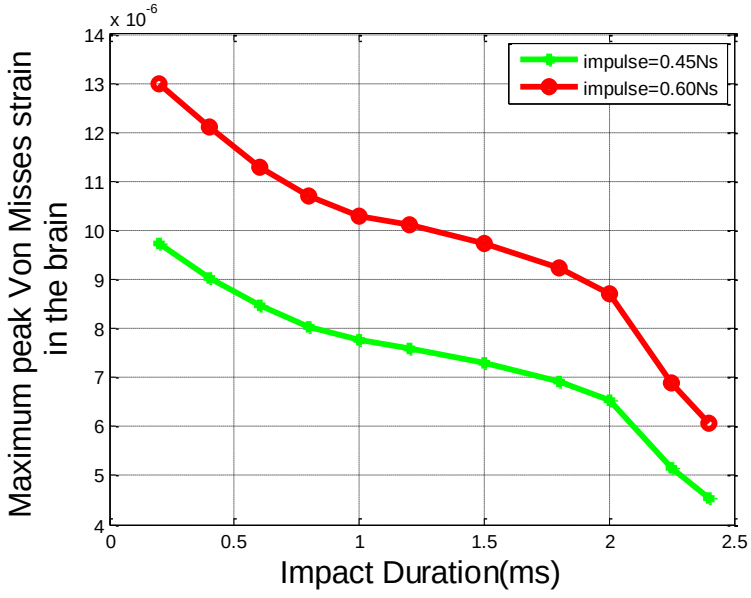

(b)

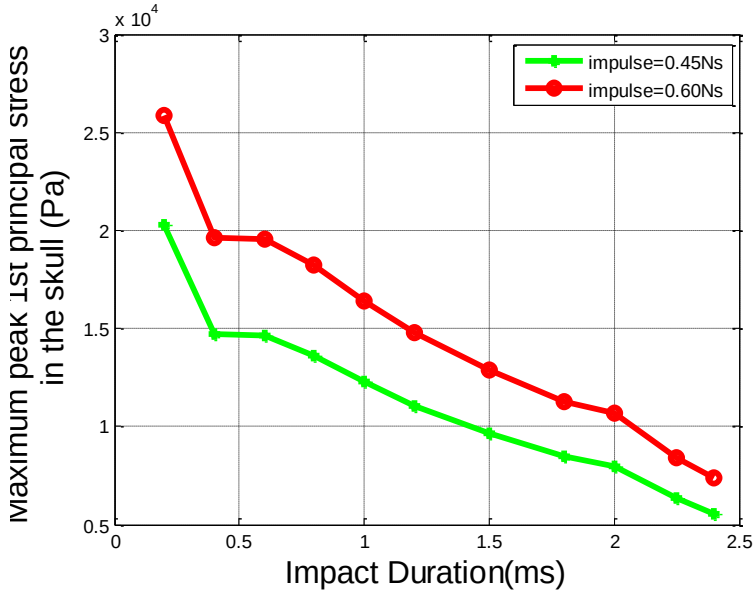

(c)

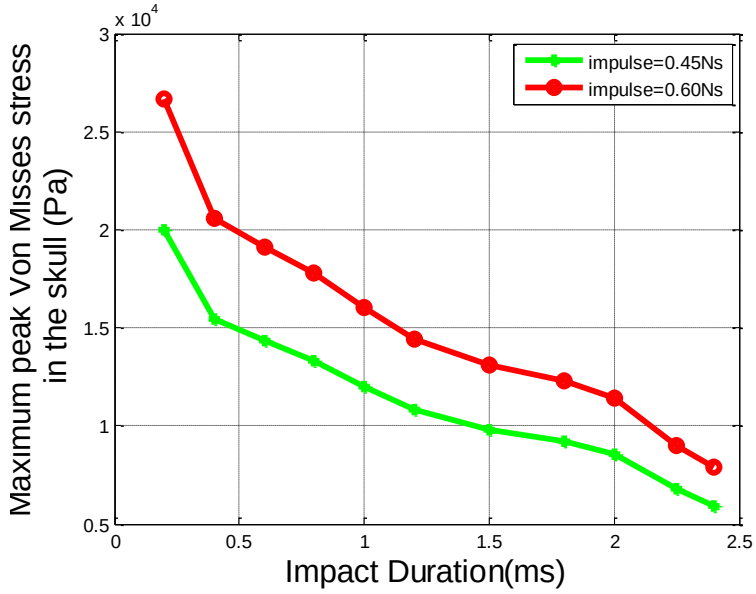

(d)

Figure 23 (a) Maximum peak 1st principal strain in the brain;

(b) Maximum peak von Misses strain in the brain;

(c) Maximum peak 1st principal stress in the skull;

(d) Maximum peak von Misses stress in the skull

Table 7. Deduction percentage of maximum peak strain and stress values

Mechanical Response \ Impulse	0.45Ns	0.6Ns
Maximum peak 1st principal strain in the brain	62.2%	52.0%
Maximum peak Von Misses strain in the brain	53.4%	53.4%
Maximum peak 1st principal stress in the skull	72.6%	71.3%
Maximum peak von stress in the skull	70.2%	70.2%

The following observations can be made from the results shown in Figure 23 and in Table 7:

1. Impact duration has significant effect on maximum peak strains in the brain. With impact duration increased from 0.2 ms to 2.4 ms, maximum peak 1st principal strain in the brain was reduced by 62.2% under impulse of 0.45Ns, and 52.0% under impulse 0.6Ns. The trend indicates that increases in impact duration will lead to further decreases in the strains.
2. The effect of impact duration on stresses in the skull is even larger. With impact duration increased from 0.2 ms to 2.4 ms, maximum peak 1st principal stress was reduced by more than 70%. The effect of impact duration is nearly independent of the input impulse.

Based on the obtained simulation results, increasing impact duration is the most effective way to reduce maximum peak strains in the brain compared with the other factors. It is also very effective for reducing stresses in the skull. The padding layer of a helmet has the functionality of changing the duration of the impact force transferred to the skull. By selecting a proper padding material for a helmet, it is possible to control the duration of impact force acting on the skull.

The investigation results obtained in Sections 4.1 ~ 4.4 may help design more effective protective helmets. First of all, if a layer of fluid can be included between the helmet shell and the padding layer, the total mechanical energy transferred to the brain would be significantly reduced. A helmet has the role of distributing an impact force to a larger area and increasing impact duration. Its outer hard shell has the equivalent effect of increasing elasticity modulus of protective layers. Changes in elasticity modulus of the shell, impact contact area and impact duration can significantly affect strains in the brain induced by impacts. Proper control of these factors would lead to remarkable reductions of strains in the brain. However, each factor has its own unique way on affecting strains in the brain. The relationships are neither simply linear nor easily described by functions. The finite element method is undoubtedly the most economical and reliable way to find out the relationships.

Chapter 5

Concluding Remarks and Future Work

5.1 Concluding Remarks

Based on the surveys and studies on HI, CHI is one of the most critical problems need to be solved to reduce the danger of HI to human health. However, the principle and the process of CHI are still not thoroughly understood. Experimental method for the study of CHI is hard to be carried out, as the harmful experiments on living human brains is forbidden. On the other hand, FEM simulation is considered as a more practical method to study CHI.

According to the studies on anatomical structure of the human head, it was found that the human head is a solid-fluid coupling structure rather than a pure solid structure. As a new contribution to head injury research field, the fluid component in the human head, CSF, was studied by comparing two FE models. According to the obtained simulation results, the maximum strain values in the brain from the model with fluid component could be

less than, the effect of CSF to strains in the brain is un-negligible and related to the external impact.

Using the fluid-solid combined FE model, three factors affecting CHI, the cranium elasticity modulus, impact contact area and impact duration, were also investigated. According to the simulation results, increasing these factors are very helpful to reduce the maximum peak strain values in the brain. Increasing the impact duration is found the most effective measure, while increasing the equivalent cranium elasticity modulus is very effective to protect the children from CHI.

By analysing the results, it was found that a fluid could provide better cushion than the solid with same material parameters. For this reason, better protection could be provided if the padding material of a helmet is made from a fluid-solid mixed material other than totally solid. This conclusion deserves a further study. Our simulation results showed that the helmets are also helpful to protect people from CHI. Conclusions obtained from the investigations are very helpful for improving the effectiveness of protective helmets.

The above studies were based on a number of assumptions. Rigid body motions of the head were constrained. The resulting problem was thus a small displacement problem. Linear material properties were also adopted. These assumptions greatly simplified the problem.

For the future work, the studies on the human head under impacts will allow large displacements. The study will be extended to a non-linear problem. To obtain more realistic simulation results, the FE model is required to be very faithful to the real human head. Moreover, the boundary conditions also need to be improved.

5.2 Further Work

Based on the previous discussions, construction of an accurate 3D FE model of human head is the major work of further research. It is believed that an accurate FE model can be built using modern medical imaging technologies. The possibility of building a 3D FE model is discussed in the following.

5.2.1 Building a three dimensional model

As discussed in Chapter 3, MR images will still be chosen as the basic data, from which geometry of the head structure and its components will extracted to build the 3D model. Commercial medical image processing software such as 3D-DOCTOR and MIMICS is able to build a 3D geometric model directly from MRI slices or other medical images. Medical image processing software supports has the functionalities such as image segmentation, calculating 3D volume and other 3D measurements for quantitative analysis.

A finite element mesh can be exported from image processing software for input into finite element analysis software [68, 69].

5.2.2 Point-by-point material properties

MRE (Magnetic Resonance Elastography) is a non-invasive method for measuring tissue elasticity. It uses MRI imaging techniques combined with an external mechanical compression to obtain an image of propagating waves through an organ [70]. Propagation pattern of mechanical waves can be used for quantitatively estimating elasticity of the medium. Mechanical waves propagate through tissues at different velocities, depending on tissue elasticity. In a stiffer material, wave velocity is faster. By detecting the wave velocity field, it is possible to determine point-by-point material elasticity.

Bibliography

[1] John Bruns Jr.and W. Allen Hauser. The epidemiology of traumatic brain injury: A review. *Epilepsia*, 44(10):2 – 10, 2003.

[2] Brain damage coup and countrecoup injury. Available from: http://www. brain-damageattorneys. com/topics.cfm/coup-contrecoup-injury.

[3] Mau-Roung Lin and Jess F. Kraus. A review of risk factors and patterns of motor-cycle injuries. *Accident analysis and prevention,*, 41(4):710 – 722, July 2009.

[4] Y. Luo, Q. Zhang, and M.D. Bigio. Recent progress in application of fem in study of non-penetrating brain injuries. *In Adv. Theor. Appl. Mech.*, 1(5):225–240, 2008.

[5] M.Bernabeu, A.Demirtas Tatlidede, E. Opisso, R. Lopez, J.M.Tormos, and A. Pascual Leone. Abnormal corticospinal excitability in traumatic diffuse axonal brain injury. *J Neurotrauma*, 26(12):2185 – 93, 2009.

[6] World Health Organization. *Neurological disorders: public health challenges*. WHO Press, 2006.

[7] Sherer M., Madison C.F., and Hannay H.J. A review of outcome after moderate and severe: Closed head injury with an introduction to life care planning. *JOURNAL OF HEAD TRAUMA REHABILITATION*, 15(2):767–782, Aguest 2009.

[8] Omar Halabieh and Justin Wan. Simulating mechanism of brain injury during closed head impact. *Lecture Notes in Computer Science*, 5104:107–118, 2008.

[9] Committee on Child Abuse and Neglect. Shaken baby syndrome: Rotational cranial injuriestechnical report. *PEDIATRICS*, 108(1):206–210, July 2001.

[10] Saatman K.E., Duhaime A.C., Bullock R., Maas A.I., Valadka A., Manley G.T., Workshop Scientific Team, and Advisory Panel Members. Classification of traumatic brain injury for targeted therapies. *JOURNAL OF NEUROTRAUMA*, 25:719 – 738, July 2008.

[11] Lindenberg R.and Freytag E. The mechanism of cerebral contusions. *AMA Archives of Pathology*, 69:440–469, 1960.

[12] M.D. W.Ritohie Russell. Cerebral involvement in head injury: A study based on the examination of two hundred russell. *Brain*, 55:549–603, 1932.

[13] Laura B. Drew and William E.Drew. The contrecoup-coup phenomenon: A new understanding of the mechanism of closed head injury. *Neurocritical Care*, 1(3):385–390, Sep 2004.

[14] Goldsmith W. The state of head injury biomechanics: past, present, and future: part 1. *Crit Rev Biomed Eng.*, 29:441–600, 2001.

[15] Motherway JA., Verschueren Peter, Van der Perre G, and Vander Sloten J.and Gilchrist MD. The mechanical properties of cranial bone: The effect of loading rate and cranial sampling position. *JOURNAL OF BIOMECHANICS*, 42:2129–2135, 2009.

[16] James H. Mcelhaney, John L. Fogle, John W. Melvin, R.R. Haynes, V. L. RobertsS., and N.M. Alem. Mechanical properties of cranial bone. *JOURNAL OF BIO-MECHANICS*, 3(5):495–511, 1970.

[17] K.B. Arbogast and S.S. Margulies. Material characterization of the brainstem from oscillatory shear tests. *J. Biomech*, 31:801–807, 1998.

[18] Brands D.W., Bovendeerd P.H., Peters G.W., and Wismans J.S. The large shear strain dynamic behavior of in-vitro porcine brain tissue and the silicone gel model material. *Proceedings of the 44th Stapp Car Crash Conference, SAE 2000-01-SC17, Atlanta, GA, USA*, pages 249–260, 2000.

[19] K. Miller. Method of testing very soft biological tissues in compression. *J. Biomech*, 38:153–158, 2005.

[20] S. Cheng and L.E. Bilston. Unconfined compression of white matter. *J. Biomech*, 40:117–124, 2007.

[21] Velardi F., Fraternali F., and Angelillo M. Anisotropic constitutive equations and experimental tensile behavior of brain tissue. *Biomech. Model. Mechanobiol*, 5:53–61, 2006.

[22] K. Miller and K. Chinzei. Mechanical properties of brain tissue in tension. *J. Biomech*, 35:483–490, 2002.

[23] E.K. Franke. The response of human skull to mechanical vibrations. Technical report, Technical Report WADC Tech. Rept. 54-24, Wright-Patterson Air Force Base, OhioWright-Patterson Air Force Base, 1954.

[24] J. D.Chalupnik, C. H. Daly, and H. C.Merchant. Material properties of cerebral blood vessels. *Final Report on Contract No. NIH-69-2232, Report No. ME 71-11, Univ. of Washington, Seattl*, 1971.

[25] Steiger H. J.and Aaslid R.and Keller S. and Reulen H. J. Strength, elasticity and viscoelastic properties of cerebral aneurysms. *Heart Vessels*, 5:41–46, 1989.

[26] Lo ̈wenhielm P. Dynamic properties of the parasagittal bridging veins. *Z. Rechtsmed*, 74:55–62, 1974.

[27] Chun Zhou, Tawfik B., and Albert I.King. Shear stress distribution in the procine brain due to rotational impact. *38th Stapp Car Crash Conf. Proc*, pages 133–143, 1994.

[28] Gilchrist M. and O'Donoghue D. Simulation of the development of frontal head impact injury. *Computational Mechanics*, pages 229 – 235, 2000.

[29] Goldsmith W. and Monson K. L. The state of head injury biomechanics: Past, present, and future. part 2: Physical experimentation. *Critical Reviews in Biomedical Engineering*, 1:105–207, 2005.

[30] A .K. Ommaya, W. Goldsmith, and L.Thibault. Head and neck injury criteria and tolerance levels. *Biomechanics and neuropathology of adult and paediatric head injury*, 16:220–242, 2002.

[31] H.and Lu C. Gong, S.and Lee. Computational simulation of the human head response to non-contact impact. *Computers and Structures,*, 86:758 – 770, 2008.

[32] Zhaoxia Li and Yunhua Luo. Finite element study of correlation between intracranial pressure and external vibration responses of human head. *Adv. Theor. Appl. Mech.*, 3(3):139–149, 2010.

[33] R. Willinger and D. Baumgartner. Numerical and physical modelling of the human head under impact - towards new injury criteria. *International Journal of Vehicle Design*, 32:940115, 2003.

[34] K. Kormi and R.A. Etheridge. Application of finite-element method to simulation of damage to the human skull as a consequence missile impact on a multi-layered composite crash helmet. *J. Bimed Eng*, 14:203–208, May 1992.

[35] Aare M. and Kleiven. S. Evaluation of head response to ballistic helmet impacts using the finite element method. *International Journal of Impact Engineering*, 34:596–608, 2007.

[36] Khalil T.B. and Hubbard R.P. Parameters study of head response by finite element modelling. *J. Biomech.*, 10:119–132, 1977.

[37] Chan H. S. mathematical model for closed head impact. *18th Stapp Car Crash Conf. Society of Automotive Engineer, Ann arbor, Michigan*, pages 557–579, 1974.

[38] Carley Ward. Finite element models of the head and their use in brain injury research. *26th Stapp Car Crash Conf. Society of Automotive Engineers, Ann Arbor, Michigan*, pages 71–85, Feb 1982.

[39] R.R. Hosey and Y.K. Liu. A homeomorphic finite element model of the human head and neck. *Finite elements in biomechanics*, pages 379–401, 1982.

[40] J. S. Ruan, T. Khalil, and A. I. King. Dynamic response of the human head to impact by three-dimensional finite element analysis. *J. Biomech. Eng.*, 116:44–51, Feb 1994.

[41] Paul A. Taylor and Corey C. Ford. Simulation of blast-induced early-time intracranial wave physics leading to traumatic brain injury. *Journal of Biomechanical Engineering*, 131:061007(1–11), June 2009.

[42] Rough anatomical structure of human head. Available from: http://www.shutter stock.com /pic-2205272/stock-photo-x-ray-image-of-a-human-head-with-brain.html.

[43] Gallucci Massimo, Capoccia Silvia, and Catalucci Alessia. *Radiographic atlas of skull and brain anatomy*. Springer, Jan.2007.

[44] Susan S. Margulies and Kirk L. Thibault. Infant skull and suture properties: Measurements and implications for mechanisms of paediatric brain injury. *Journal of Biomechanics Engineering*, 122(12):364–371, Agu,2000.

[45] Margulies.S.S. and Coats B. Material properties of human infant skull and suture at high rates. *JOURNAL OF NEUROTRAUMA*, 23(8):1222–1232, Agu,2006.

[46] A. Gilroy, B. MacPherson, L.Ross M. Schuenke, and E. Schulte. Atlas of anatomy. *Thieme Medical Publisher, New York*, 2008.

[47] The public domain National Institute for Aging, a branch of NIH, *Alzheimers disease, unraveling the mystery*. United States Postal Service, 1978.

[48] Hrapko M., Van Dommelen J .A.and Peters GM., and JS. Wismans. The mechanical behaviour of brain tissue: Large strain response and constitutive modeling. *Biorheology*, 43:623–636, 2006.

[49] G. Franceschinia, D. Bigonia abd P. Regitnigb, and G .A. Holzapfelc. Brain tissue deforms similarly to filled elastomers and follows consolidation theory. *Journal of the Mechanics and Physics of Solids*, 54:2592–2620, Dec.2006.

[50] Miller K., Chinzei K., and Orssengo G.and Bednarz P. Mechanical properties of brain tissue in-vivo: experiment and computer simulation. *J Biomech*, 33(11):1369–76, Nov,2000.

[51] Protection of the Brain. Available from: http://legacy.owensboro.kctcs.edu/gcaplan/anat/notes/api%20notes%20l%20central%20nervous%20system-brain.htm.

[52] Ho Johsin and Kleiven Svein. Dynamic response of the brain with vasculature: A three-dimensional computational study. *Journal of Biomechanics*, 40:3006–3012, 13.

[53] Anatomical structure of artery. Available from: http://www.mdconsult.com/das/patient/ body/207786395-2/0/10041/36514.html.

[54] Kenneth L. Monson, Werner Goldsmith, Nicholas M. Barbaro, and Geoffrey T. Manley. Characterisation of the mechanical behavior of brain tissue in compression and shear. *Biorheology*, 125(2):288– 296, April 2003.

[55] Monson K., Goldsmith W., and Manley G. Static and dynamic mechanical and failure properties of human cerebral vessels. *Proceedings of the 9th Symposium on Crashworthiness occupant Protection and Biomechanics in Transportation System.New York, ASME*, 49:255–265, 2000.

[56] Kenneth L. Monson, Werner Goldsmith, Nicholas M. Barbaro, and Geoffrey T. Manley. Axial mechanical properties of fresh human cerebral blood vessels. *Journal of Biomechanical Engineering*, 125:288–294, APRIL, 2003.

[57] Allison C. Bain and David F. Meaney. Tissue-level thresholds for axonal damage in an experimental model of central nervous system white matter injury. *Journal of Bio-mechanical Engineering*, 121:615–622, Dec.2000.

[58] Axial view inside the skull. Available from: http://nautilusmedicalsystems.com/pages/services.html.

[59] Waks A. and Tretiak O.J. Recognition of regions in brain sections. *Comput Med Imaging Graph.*, 14:341–352, 1990.

[60] Dassios G., Kiriakopoulos M. K., and Kostopoulos V. On the sensitivity of the vibrational response of the human head. *Computational Mechanics*, 21(4-5):382 – 388, 1998.

[61] B.V. Mehta, R. Mulabagula, and J.Patel. Finite element analysis of the human skull considering the brain and bone material properties. *Computer Methods in Biomechanics and Biomedical Engineering*, pages 217–227, 1996.

[62] Davis J. Wave propagation in solids and fluids. *Springer-Verlag*, 1988.

[63] O. C. Zienkiewicz, R. L. Taylor, and J. Z. Zhu. The finite element method: Its basis and fundamentals. *Elsevier Butterworth-Heinemann*.

[64] Zienkiewicz O. C. and Newton R. E. Coupled vibrations of a structure submerged in a compressible fluid. *Proceedings of the Symposium on Finite Element Techniques, University of Stuttgart, Germany*, June,1969.

[65] Craggs A. A finite element model for acoustically lined small rooms. *Journal of Sound and Vibration*, Vol. 108, No. 2,:327–337, 1986.

[66] Hongxi Chen, Y. Luo. Parametric study of closed head injuries. In Adv. Theor. Appl. Mech., vol 3(7):339–347, 2010.

[67] Hongxi Chen and Yunhua Luo. Numerical Investigation of Several Factors Affecting Closed Head Injuries. *The Canadian Society for Mechanical Engineering Forum 2010, June 7-9,* 2010, Victoria, British Columbia, Canada

[68] The introduction of MIMICS. Available from: http://www.ablesw.com/3d-doctor/mriapp.html.

[69] Application of 3D-DOCTOR in human head modelling. Available from: http://www.ablesw.com/3d-doctor/mriapp.html.

[70] R. Muthupillai, D. J. Lomas, P. J. Rossman, R. L. Ehman, J. F. Greenleaf, and A. Manduca. Magnetic resonance elastography by direct visualization of propagating acoustic strain waves. *Science*, 269(5253):1854–1857, 1995.